THE CONFIGURATION AND RELATIONS OF THE PITUITARY GLAND AND FOSSA

A radiological, pathological and clinical study

VOLUME II (Figures)

MAURICE S. F. McLACHLAN
M. D., University of Edinburgh, 1971

CONTENTS

VOLUME I (Text)

VOLUME II (Figures) Page

PART I

ESTIMATION OF PITUITARY GLAND DIMENSIONS FROM RADIOGRAPHS OF THE SELLA

Figures 1 - 12

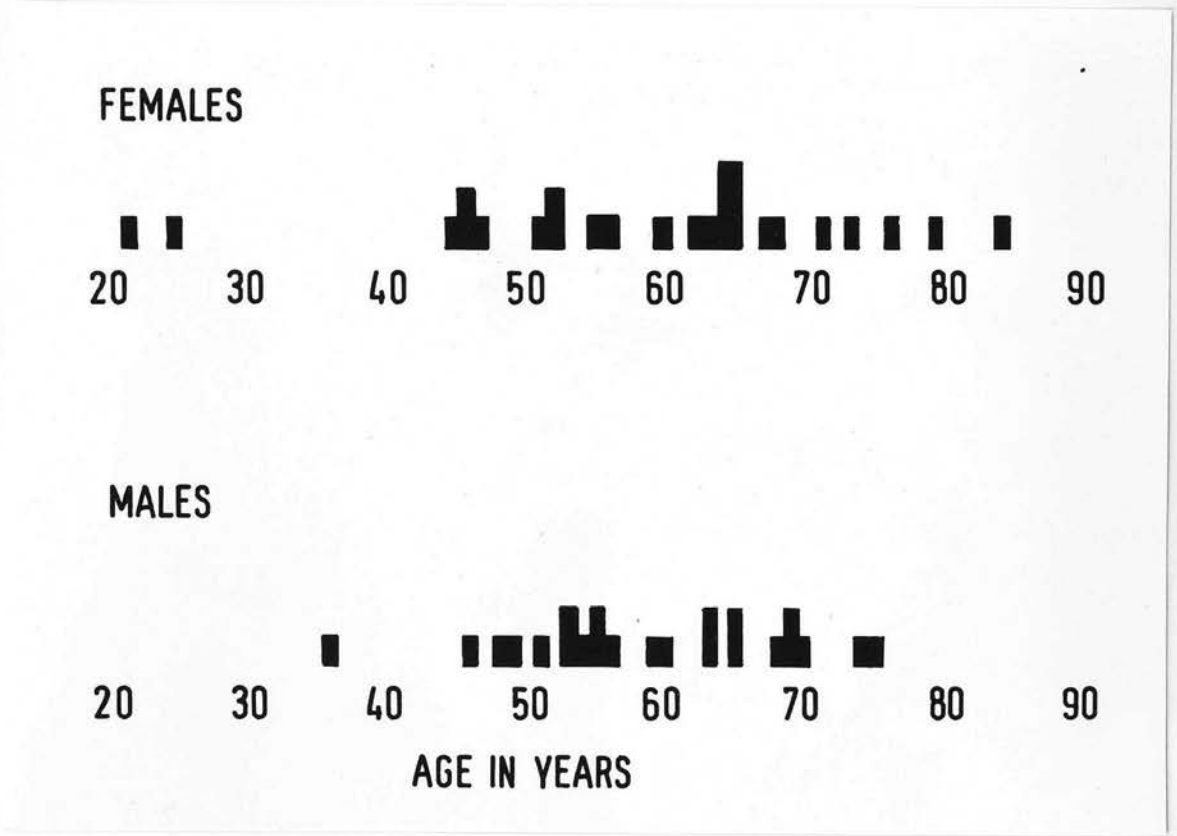

Figure 1

Age distribution in males and females in the necropsy series.

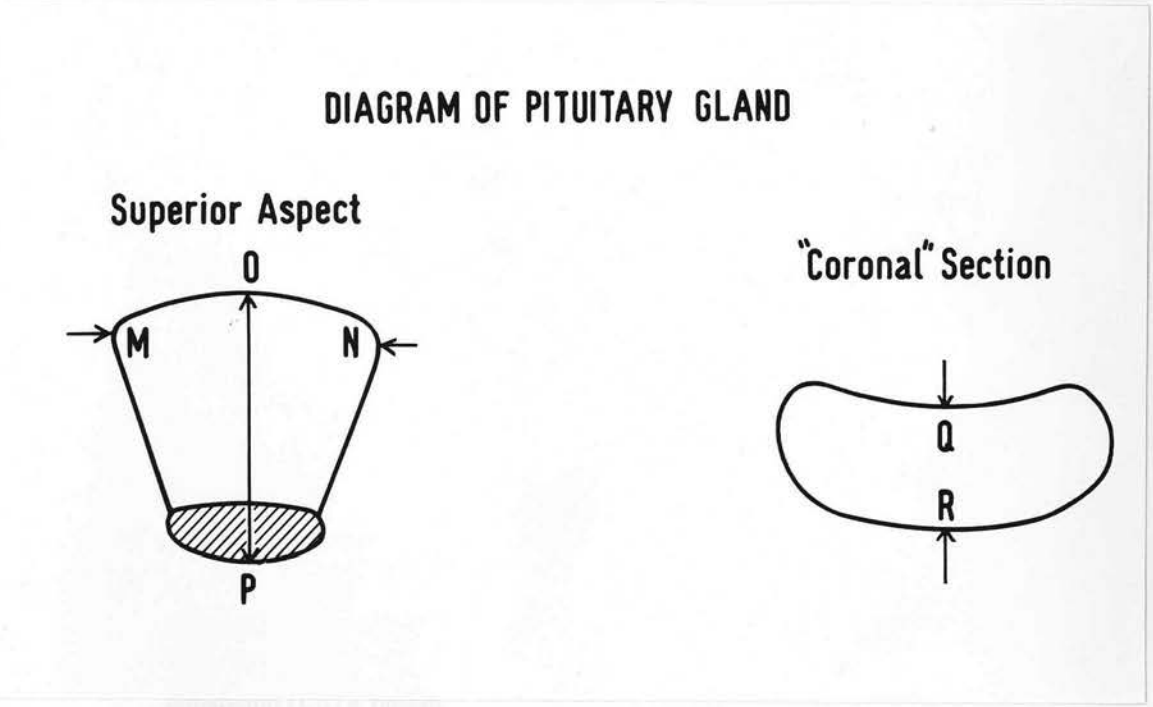

Figure 2

The shape of the pituitary gland varies considerably. The most common shape is shown. The pars posterior is shaded.

The greatest width (MN) and length (OP) were measured. Height (QR) was measured from the centre of the concavity that usually forms the superior surface of the gland. Where no concavity existed the greatest supero-inferior dimension was measured. In each case the pituitary stalk had been removed.

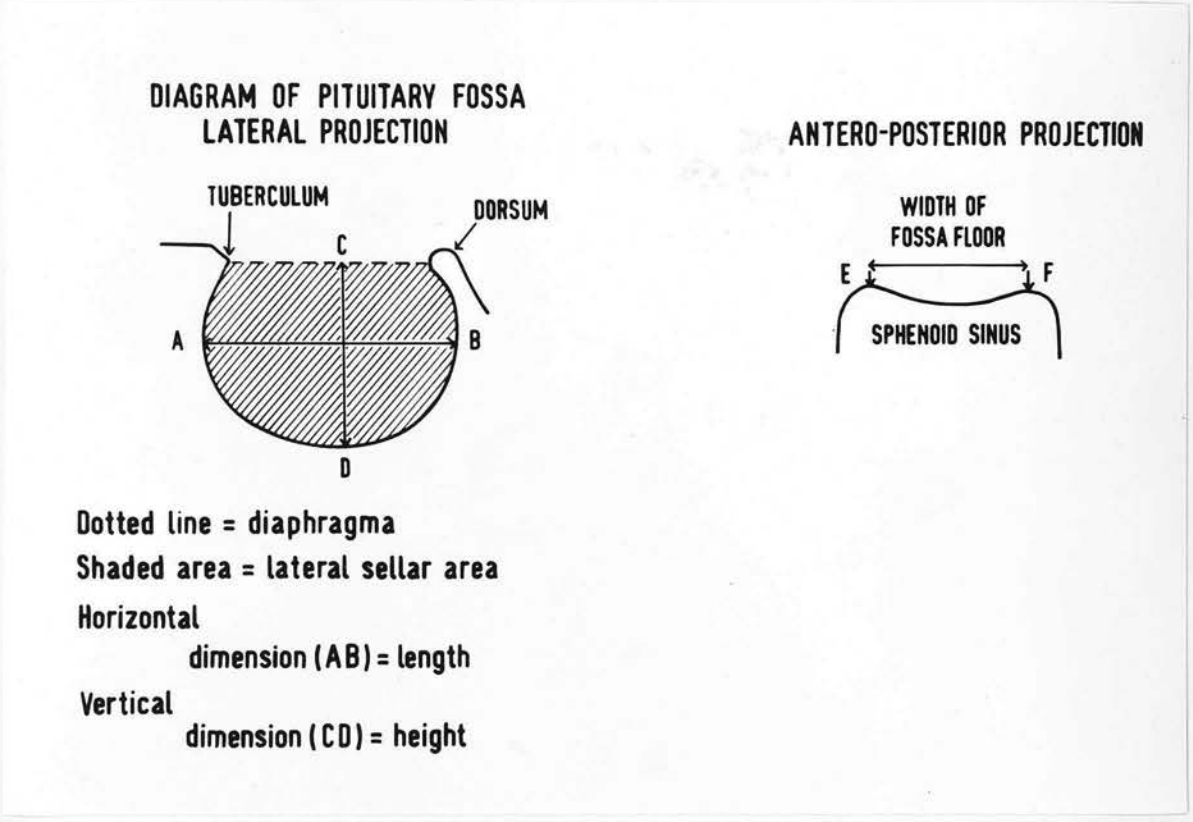

Figure 3

The line of the diaphragma (as defined here) runs from the tuberculum to the most anterior point on the convexity of the tip of the dorsum.

Length (A B) and height (C D) are, respectively, the greatest dimensions measured parallel to and at right angles to the "diaphragmatic line". Width (E F) is measured between the highest points of the lateral edges of the plateau of the fossa floor.

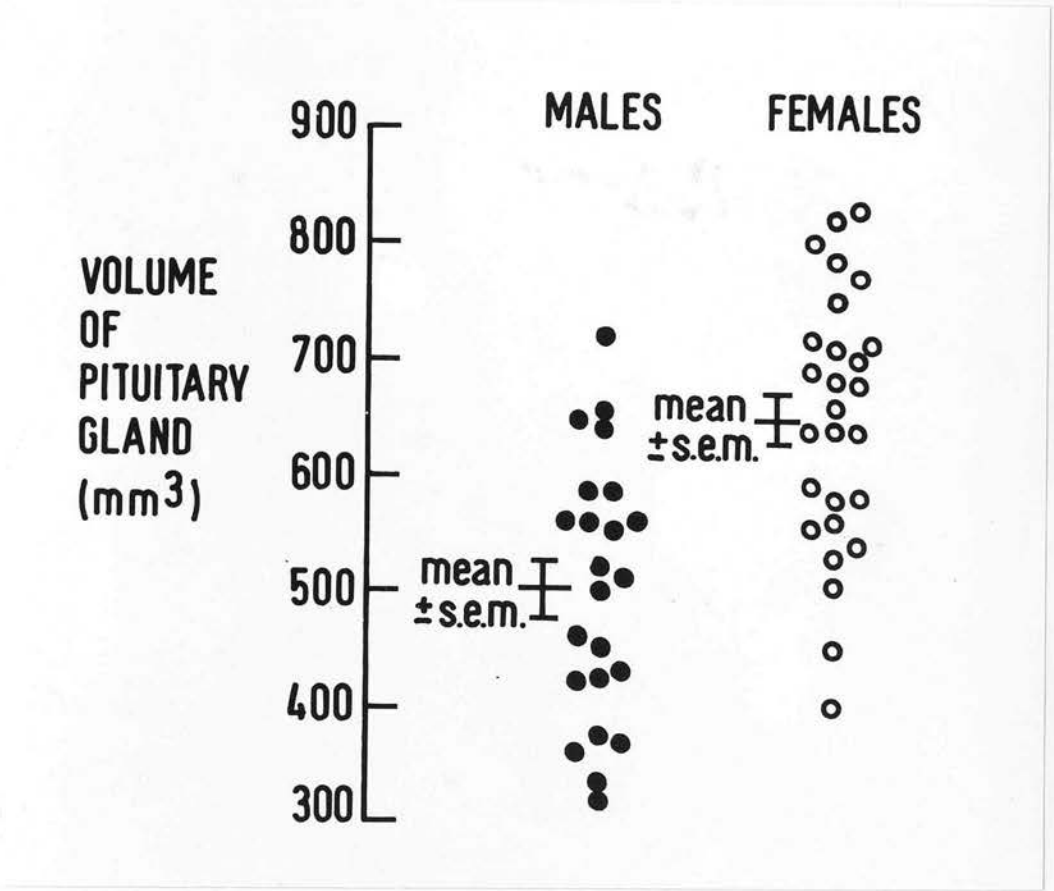

Figure 4

Pituitary gland volume plotted separately for males and females. Mean volume in females (range 399 - 827 mm^3) is 147 mm^3 greater than mean volume in males (range 320 - 718 mm^3). This difference is significant at the 0.1% level.

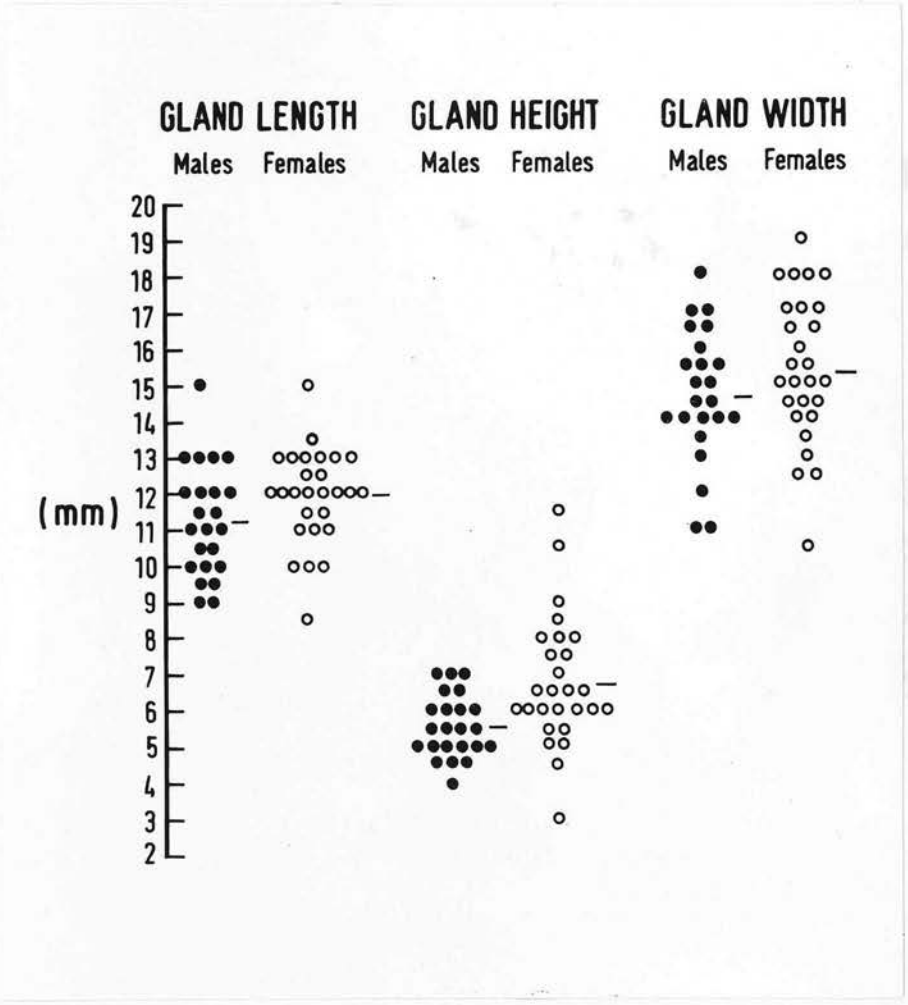

Figure 5

Linear gland dimensions (mm) plotted separately for males and females. Mean linear dimensions in the females are all slightly greater than in the males. Gland height varies more in the females than in the males. The mean in each group is shown by the horizontal line.

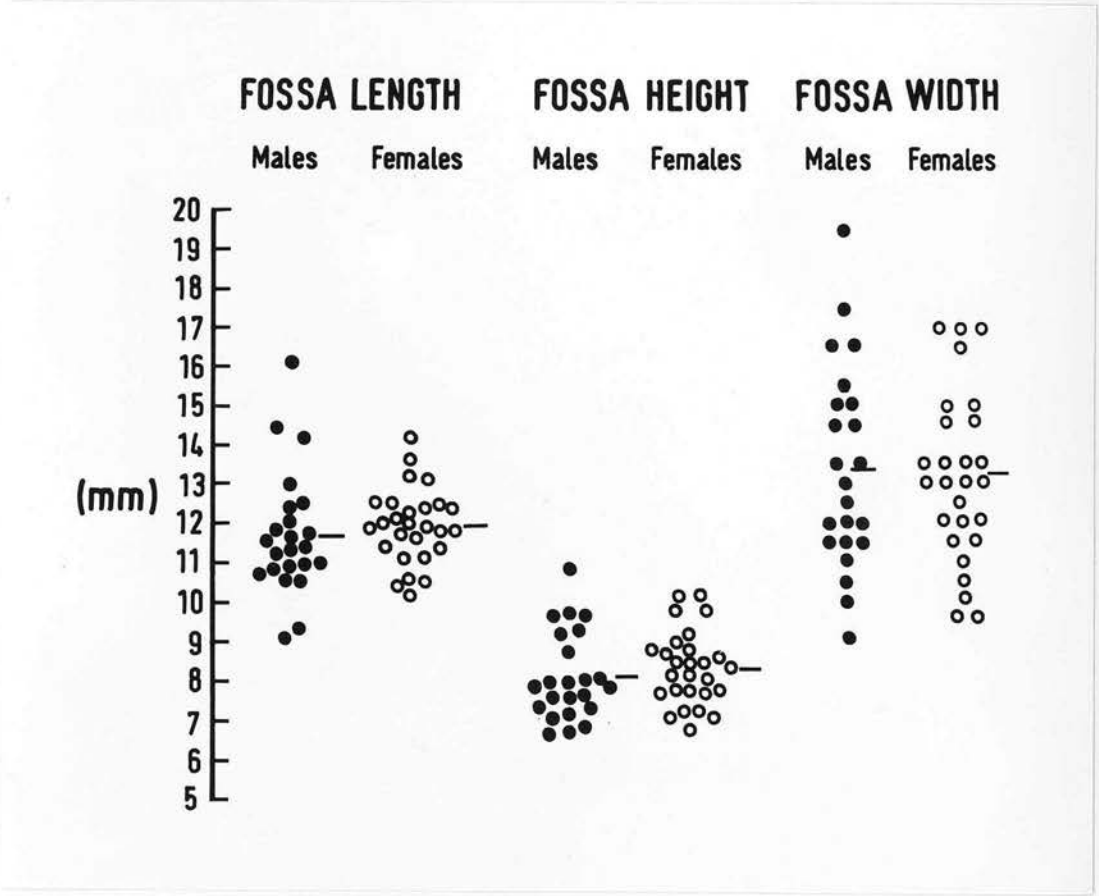

Figure 6

Linear fossa dimensions (mm), measured from radiographs, shown separately for males and females. There is no significant difference in the means. Note the relatively small variation in fossa height in the females compared with gland height shown in Fig. 5. The mean in each group is shown by the horizontal line.

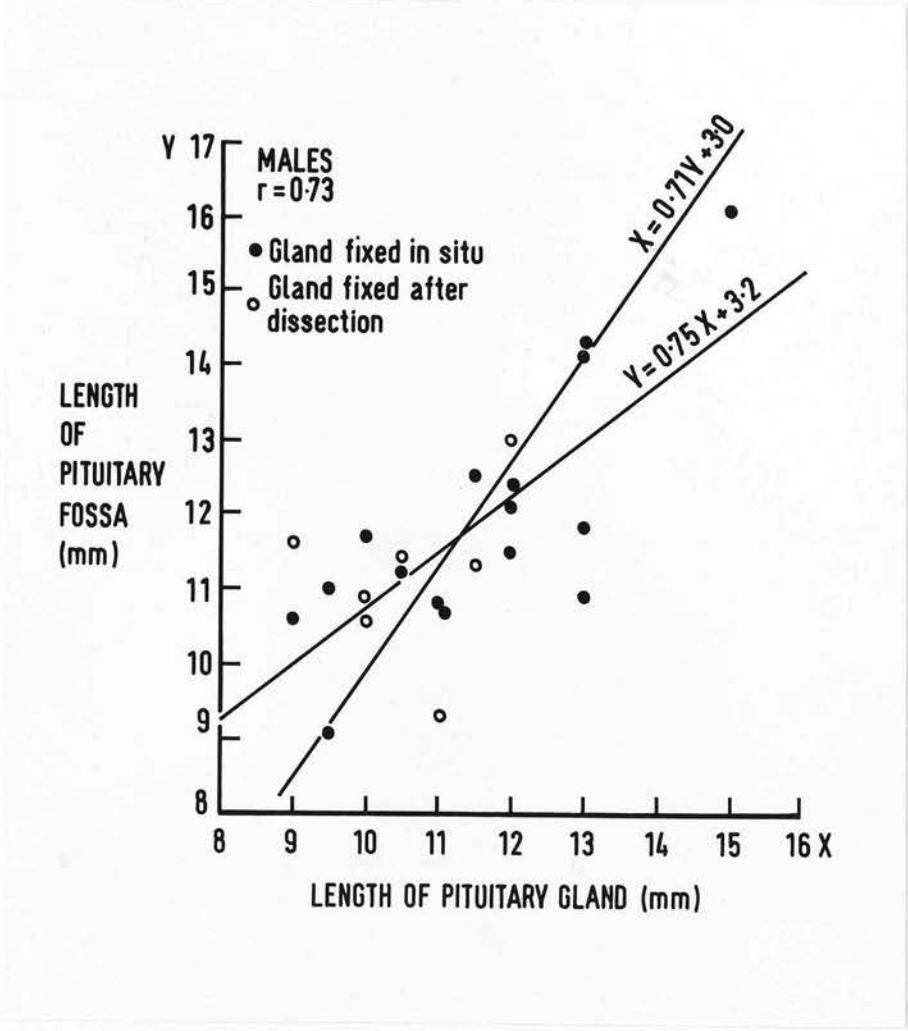

Figure 7

(a) Correlation between gland length and fossa length for males. This is good ($p < 0.001$). No differences were apparent between the glands fixed in situ and those fixed after dissection (see also Figs. 7b - 10).

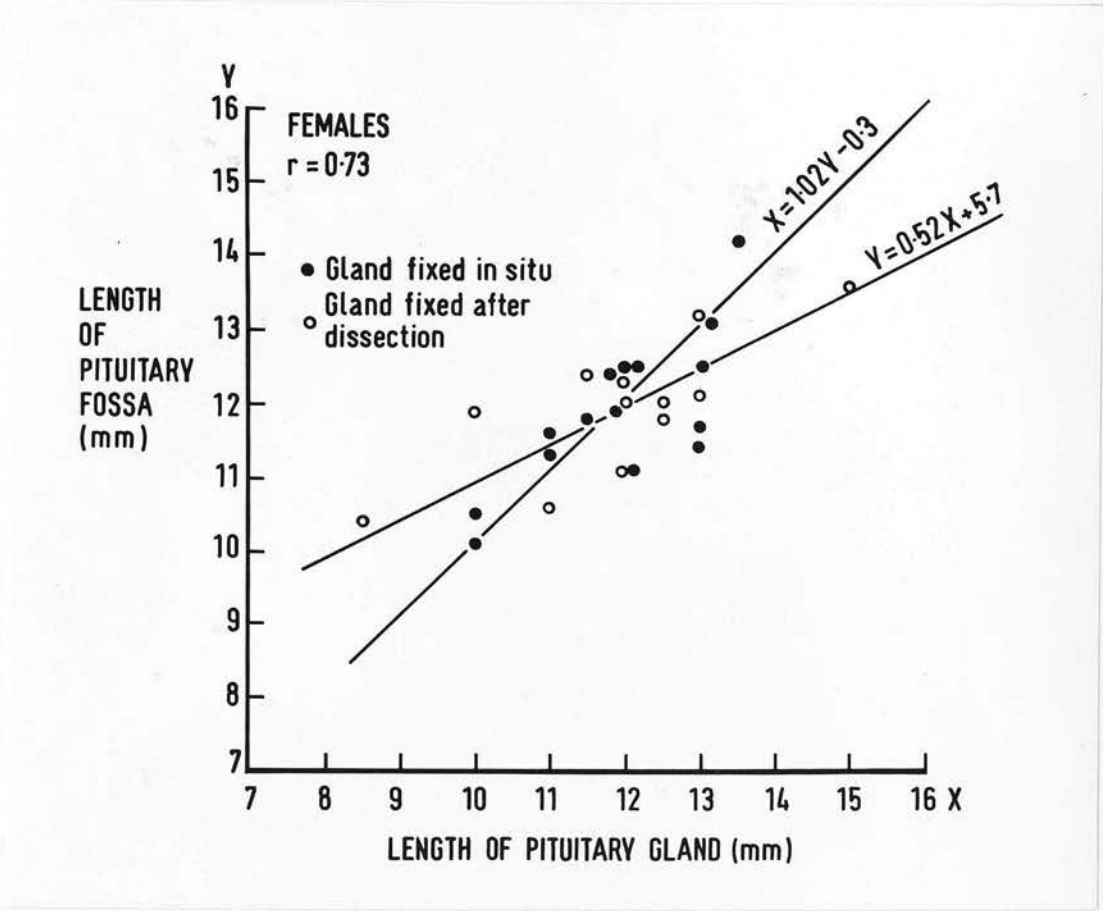

Figure 7 (cont.)

(b) Correlation between gland length and fossa length for females. As in males, this is good ($p < 0.001$).

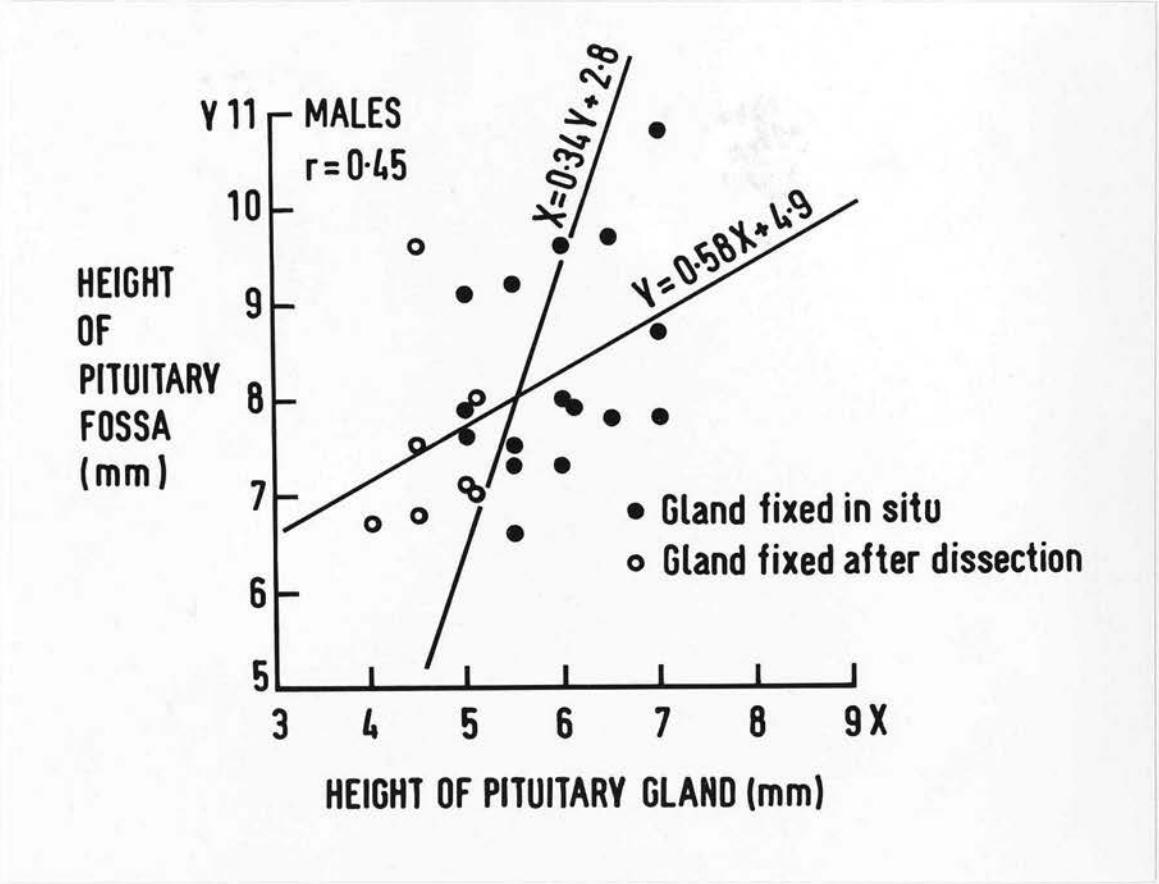

Figure 8

(a) Correlation between gland height and fossa height for males. This is poor ($p < 0.05$).

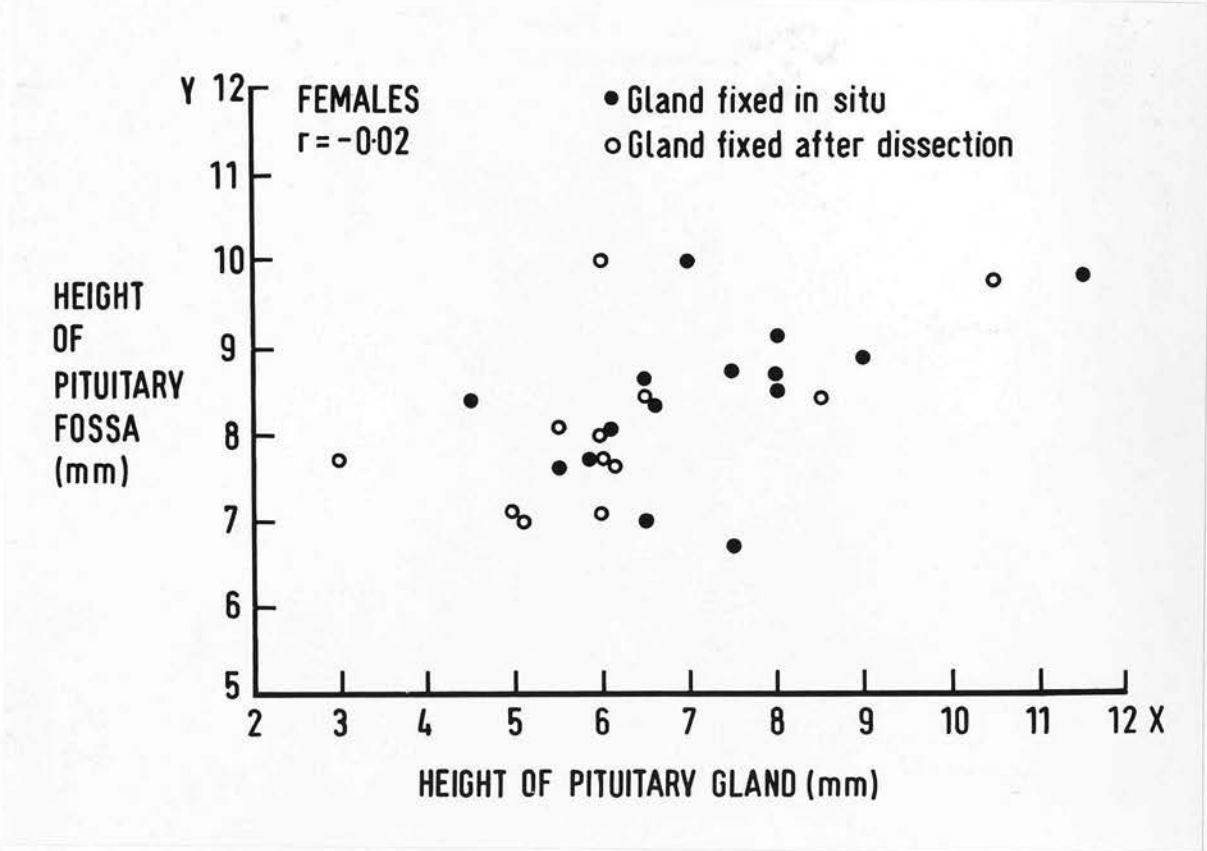

Figure 8 (cont.)

(b) Correlation between gland height and fossa height for females. No correlation exists.

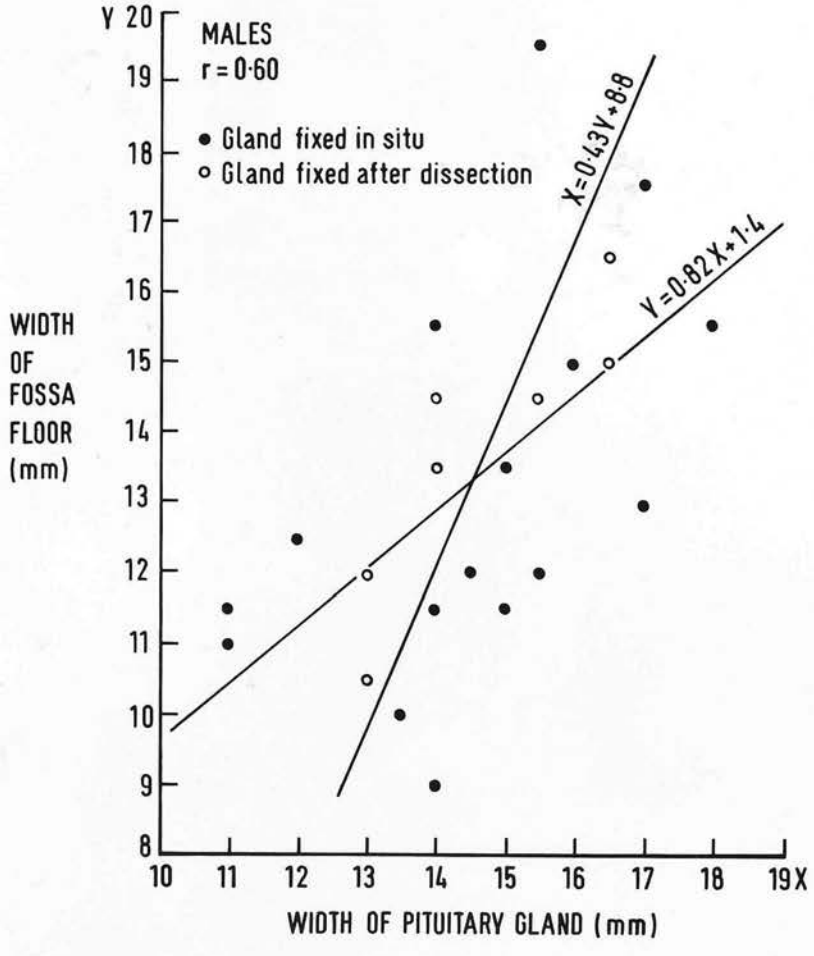

Figure 9

(a) Correlation between gland width and sellar floor width for males. This is moderately good ($p < 0.01$).

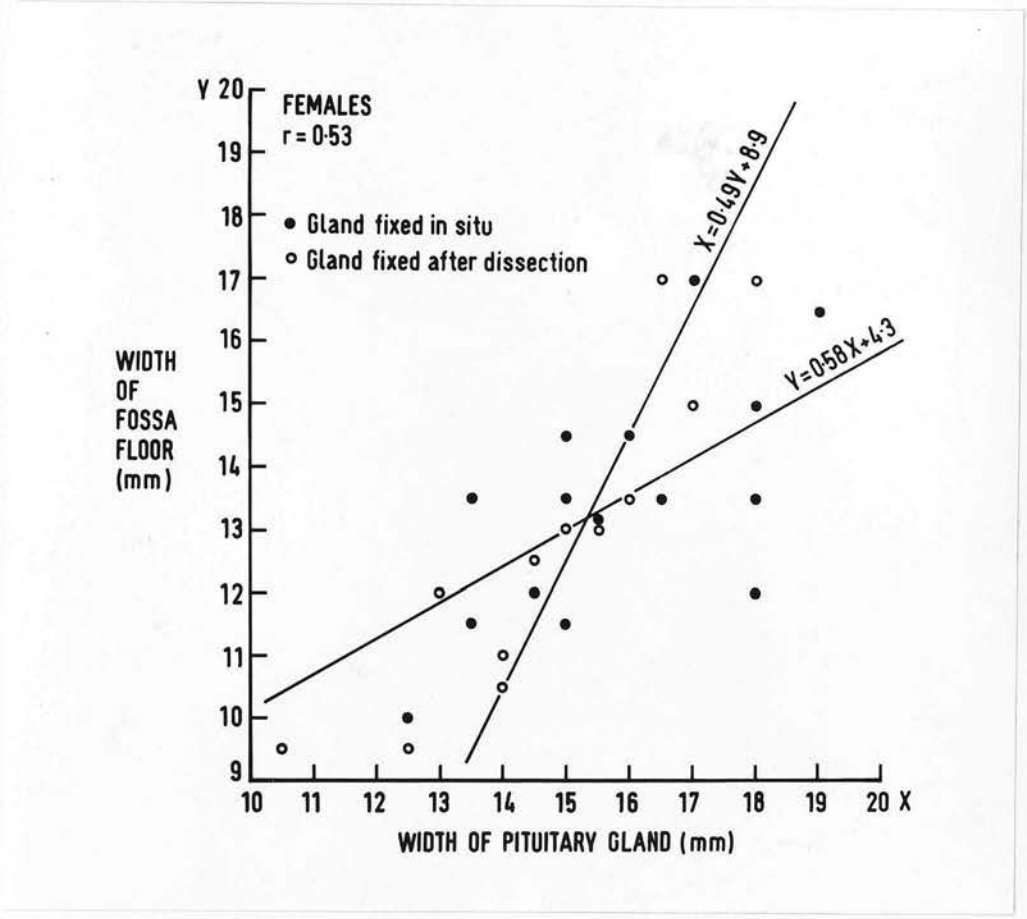

Figure 9 (cont.)

(b) Correlation between gland width and sellar floor width for females. As in males, this is moderately good ($p < 0.01$).

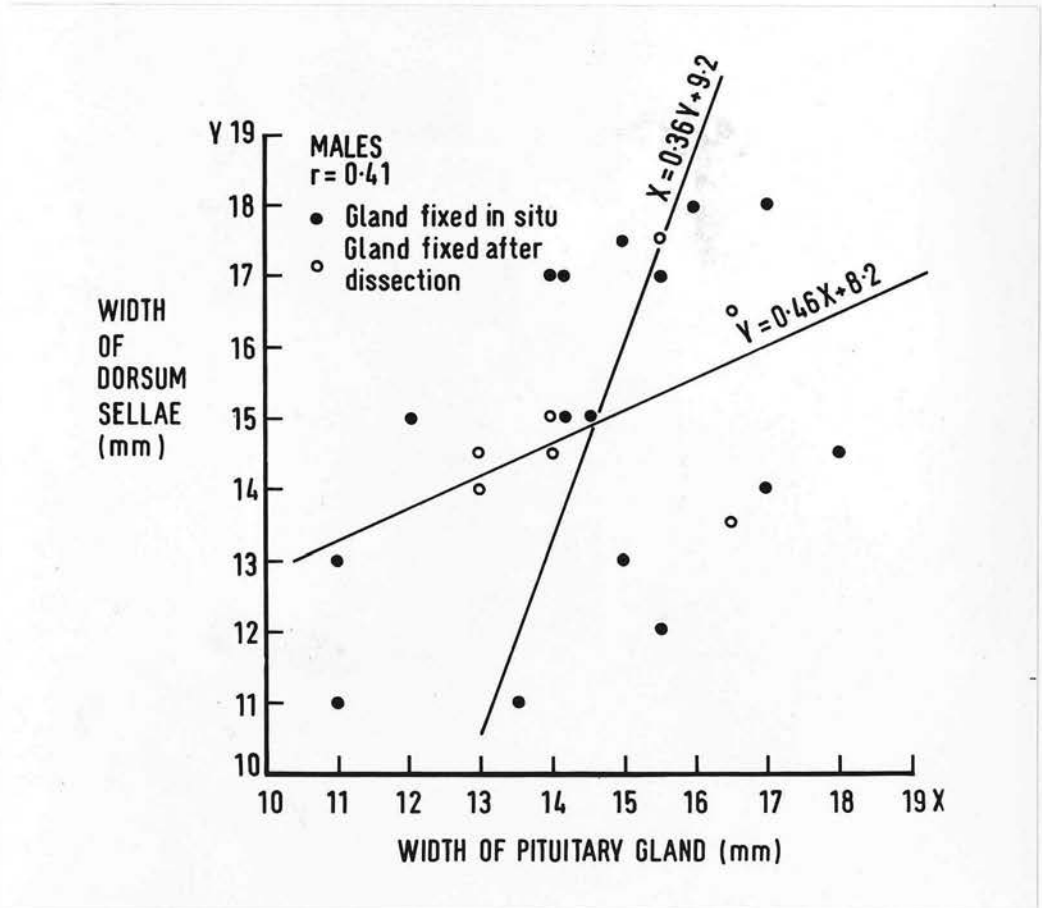

Figure 10

(a) Correlation between gland width and dorsum width for males. This is poorer than in Fig. 9a ($0.05 < p < 0.1$).

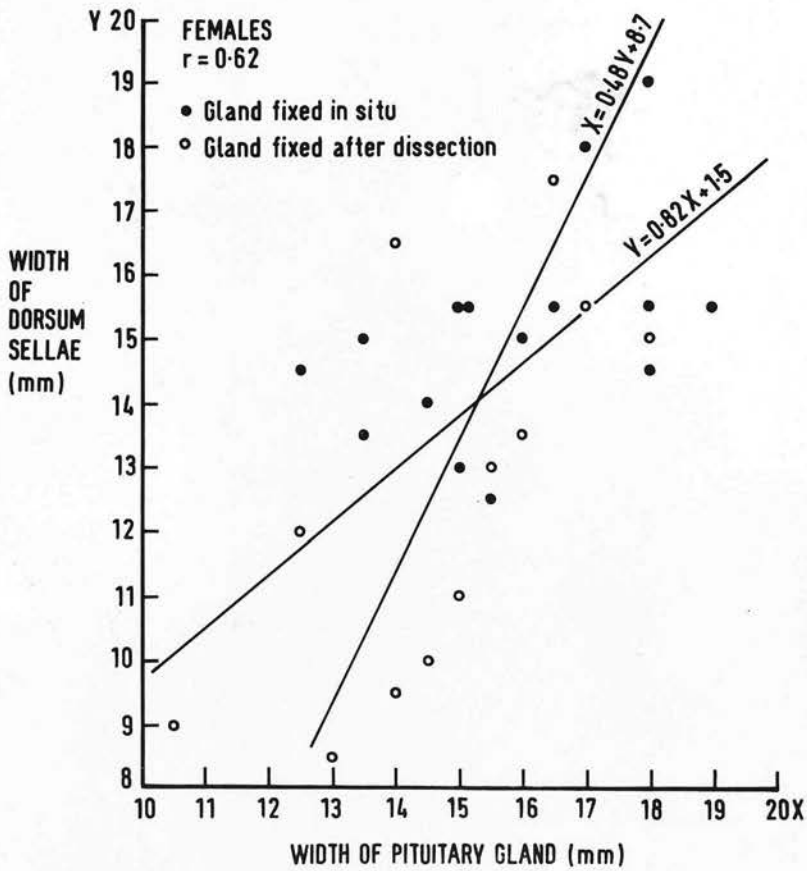

Figure 10 (cont.)

(b) Correlation between gland width and dorsum width for females. This is better than in Fig. 9b ($p < 0.001$).

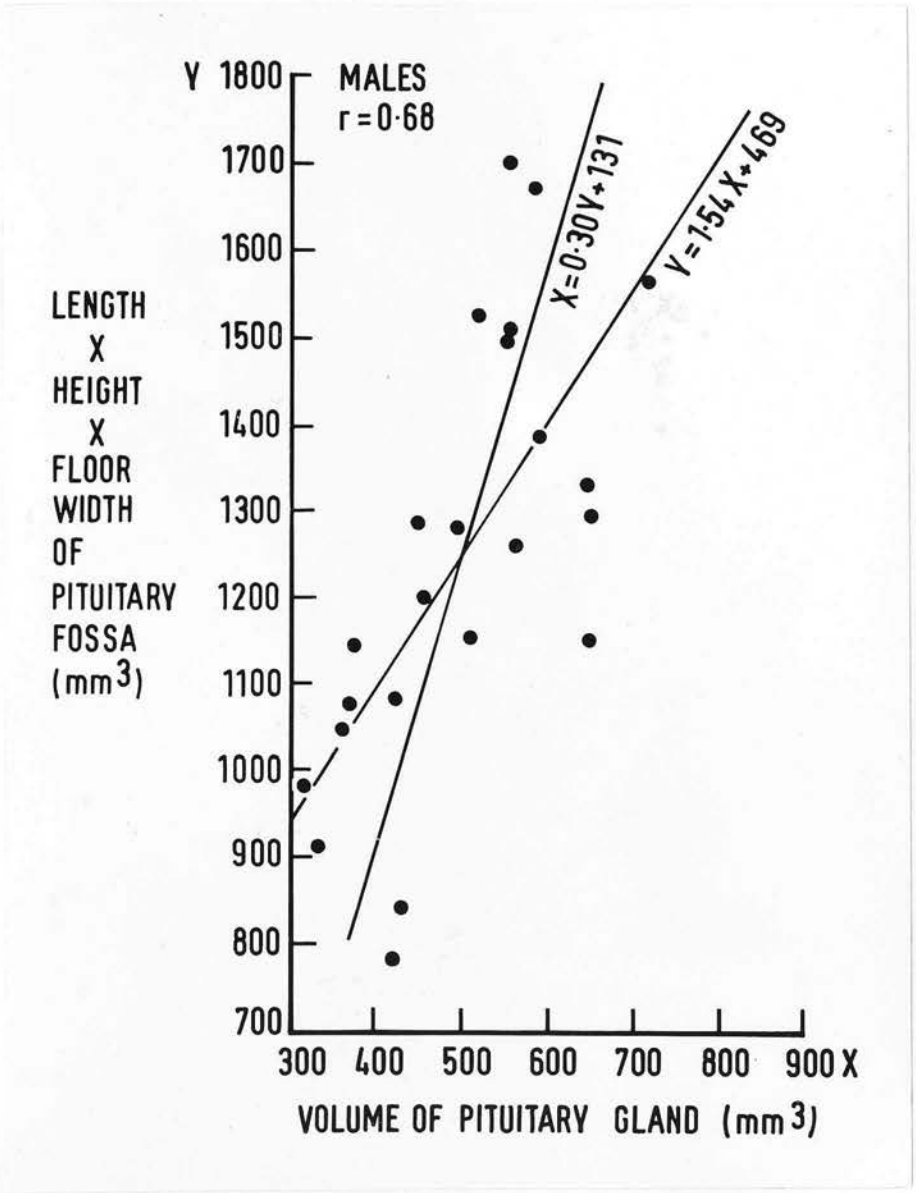

Figure 11

(a) Gland volume plotted against LxHxW for males. Correlation is good ($p < 0.001$).

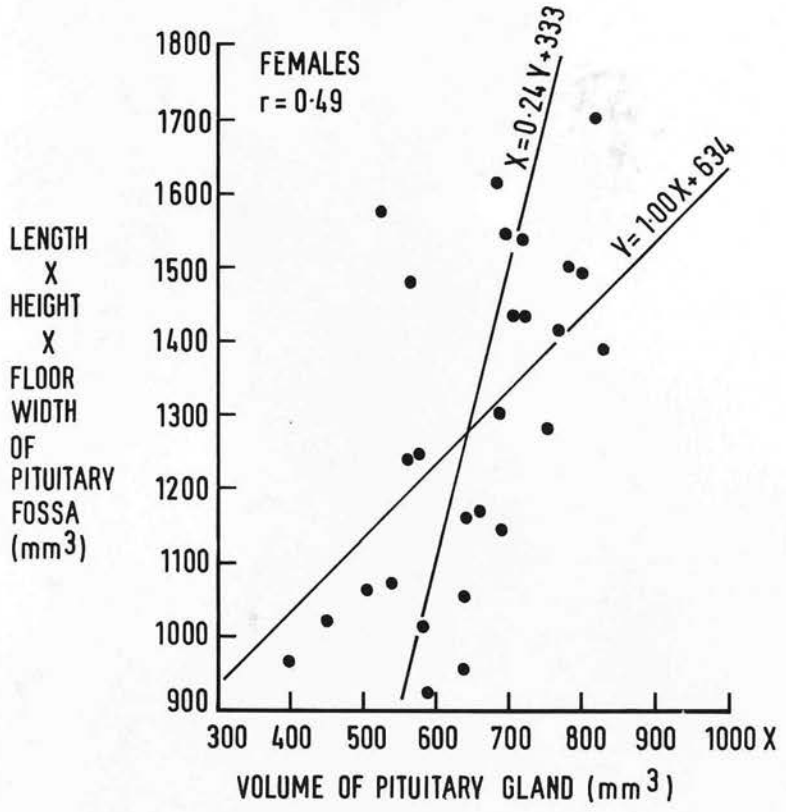

Figure 11 (cont.)

(b) Gland volume plotted against LxHxW for females. Correlation is moderately good ($p < 0.01$).

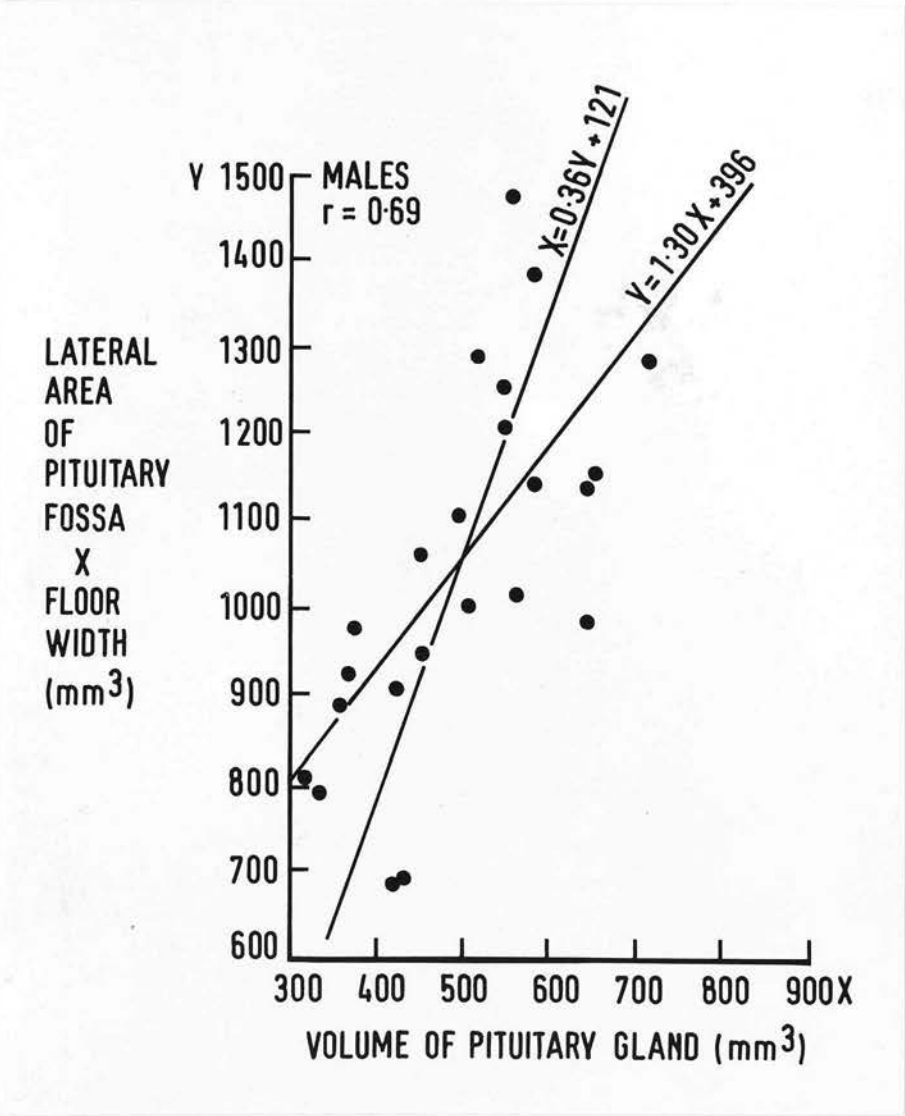

Figure 12

(a) Gland volume plotted against AxW for males. Correlation is good ($p < 0.001$).

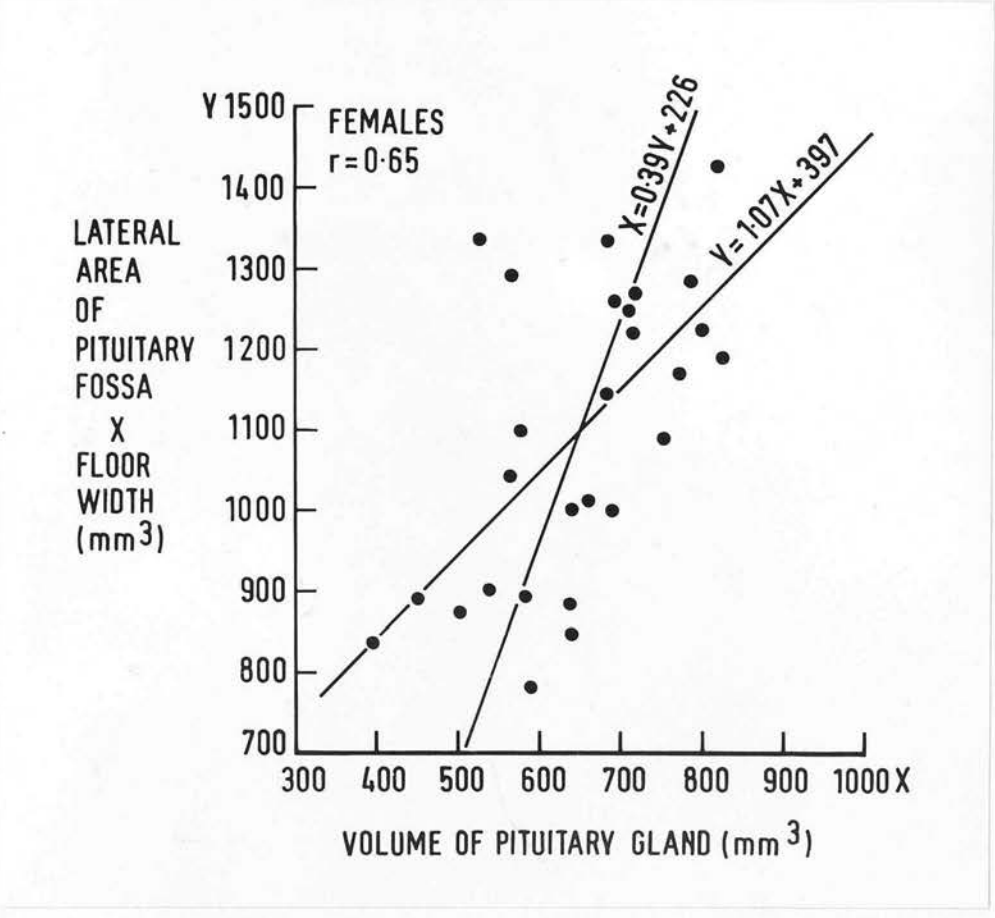

Figure 12 (cont.)

(b) Gland volume plotted against AxW for females. Correlation is good ($p < 0.001$) and is significantly better than in Fig. 11b.

PART II

CONFIGURATION OF SOFT TISSUE BOUNDARIES OF THE SELLA

Figures 13 - 28

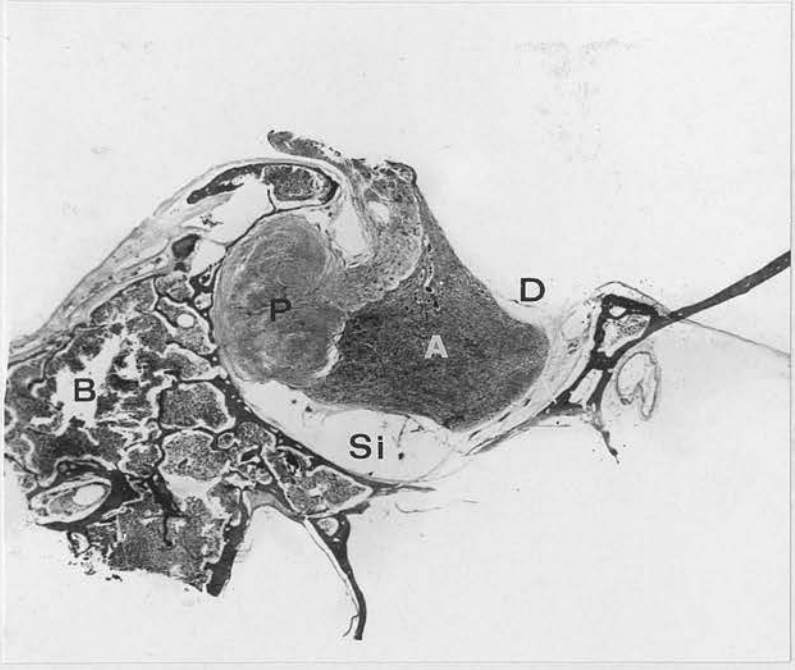

Figure 13

(a) Sagittal section through intact fossa from a female of 53 years (H & E x 4.5)

A = anterior lobe; P = posterior lobe; D = diaphragma; B = bone (sphenoid); Si = intercavernous sinus.

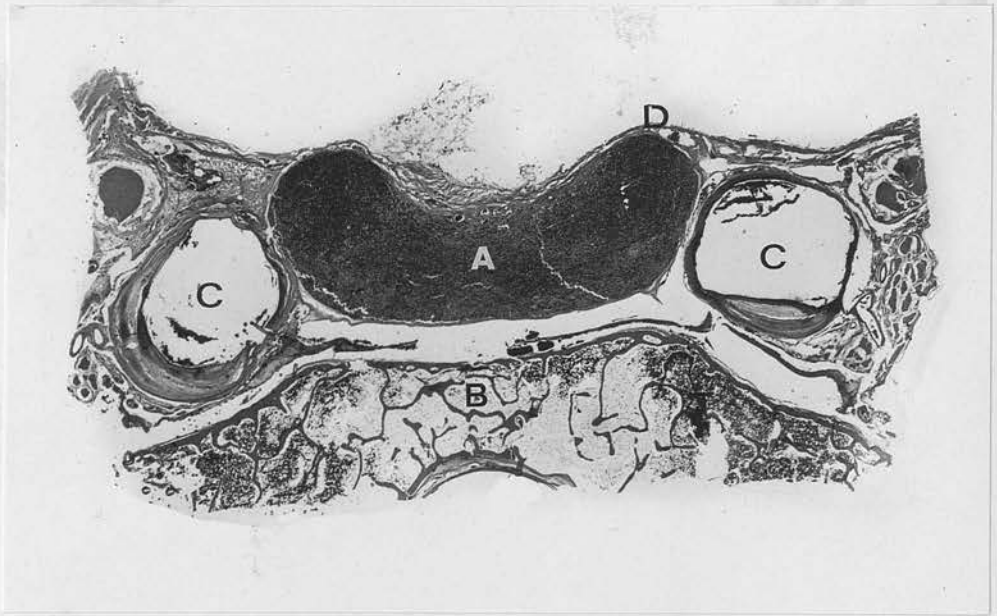

Figure 13 (cont.)

(b) Coronal section through intact fossa from a male of 44 years (H & E x 4.5)

A = anterior lobe; D = diaphragma; C = internal carotid arteries; B = bone (sphenoid).

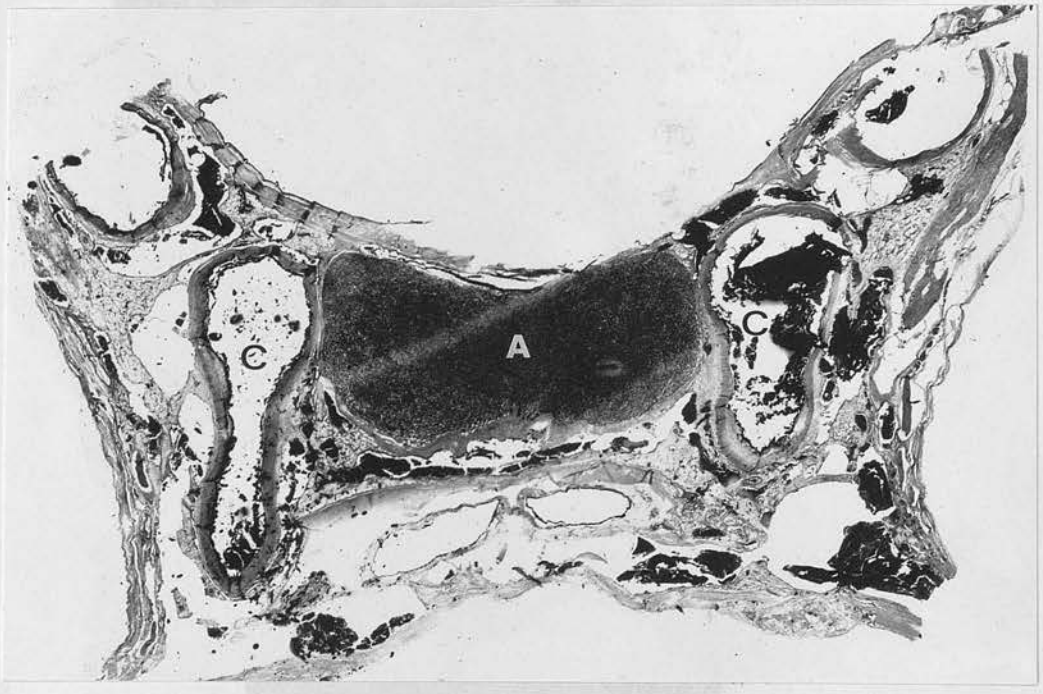

Figure 13 (cont.)

(c) Horizontal section through intact fossa from a male of 63 years (H & E x 4.5). Anterior aspect lies uppermost.

A = anterior lobe; C = internal carotid arteries.

a

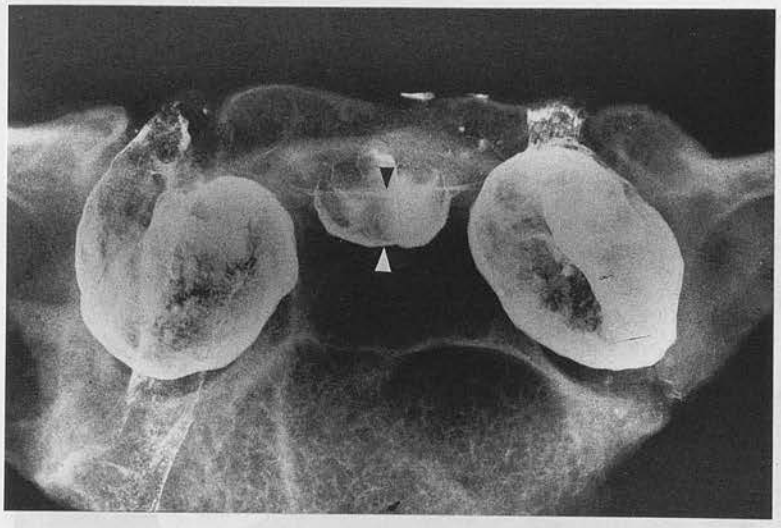

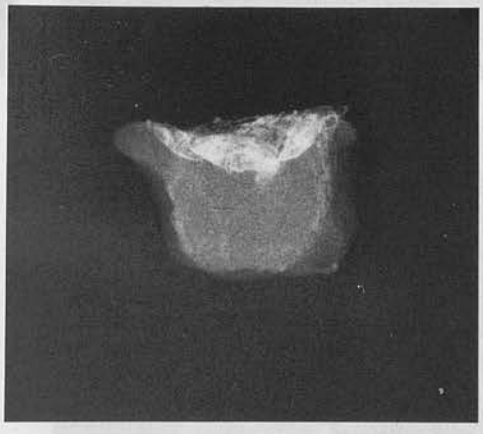

b

Figure 14

Gland compression by tortuous carotid arteries. Bismuth powder outlines the carotid siphons, the diaphragma and the upper surface of the gland.

(a) and (b) are antero-posterior radiographs of fossa and gland. The gland has been compressed laterally by tortuous, dilated arteries. A large infundibular foramen, also shown in (c), is present in the diaphragma. The upper arrow in (a) points to the diaphragma, the lower arrow to the upper surface of the gland.

c

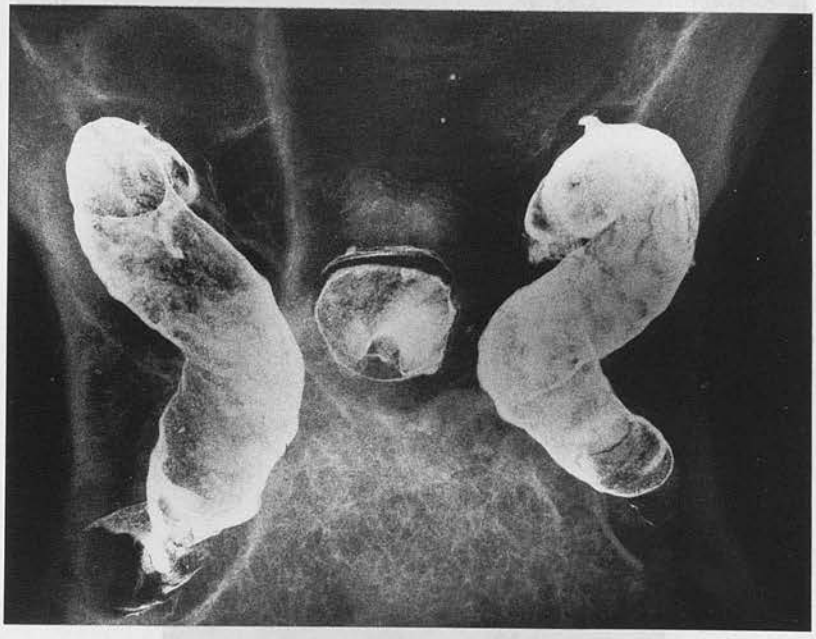

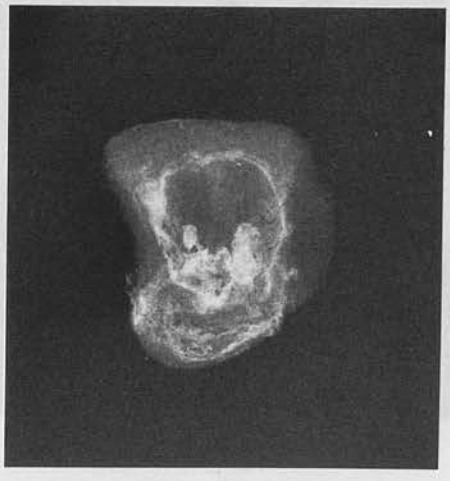

d

Figure 14 (cont.)

(c) and (d) are supero-inferior radiographs of the same fossa and gland. Lateral compression of the gland by carotid siphons is again shown. The large circular infundibular foramen is well shown in (c).

a

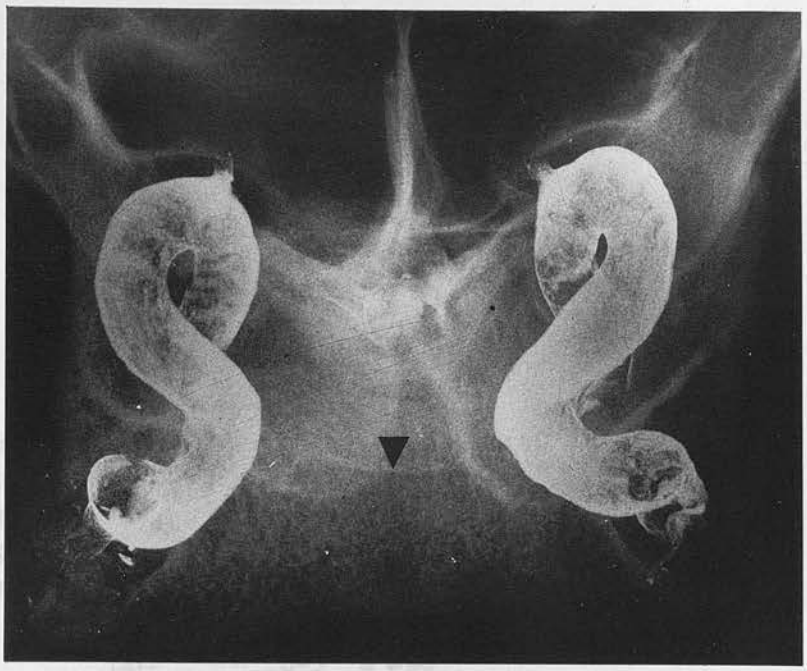

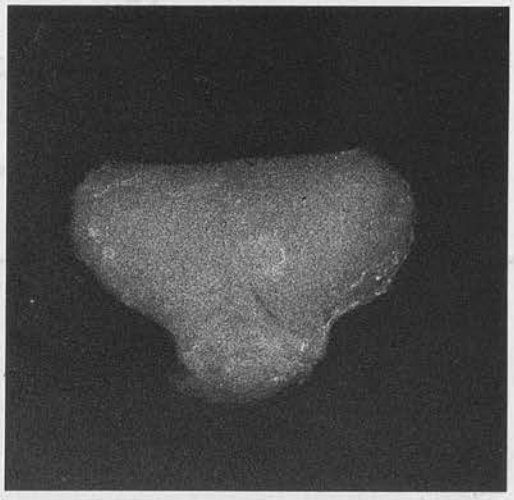

b

Figure 15

Supero-inferior radiographs of pituitary fossa (a) and gland (b). The configuration of the carotid arteries parallels the lateral contours of the gland. Maximum gland width exceeds minimum intercarotid distance by 6.5 mm in this instance. The dorsum sellae is arrowed in (a).

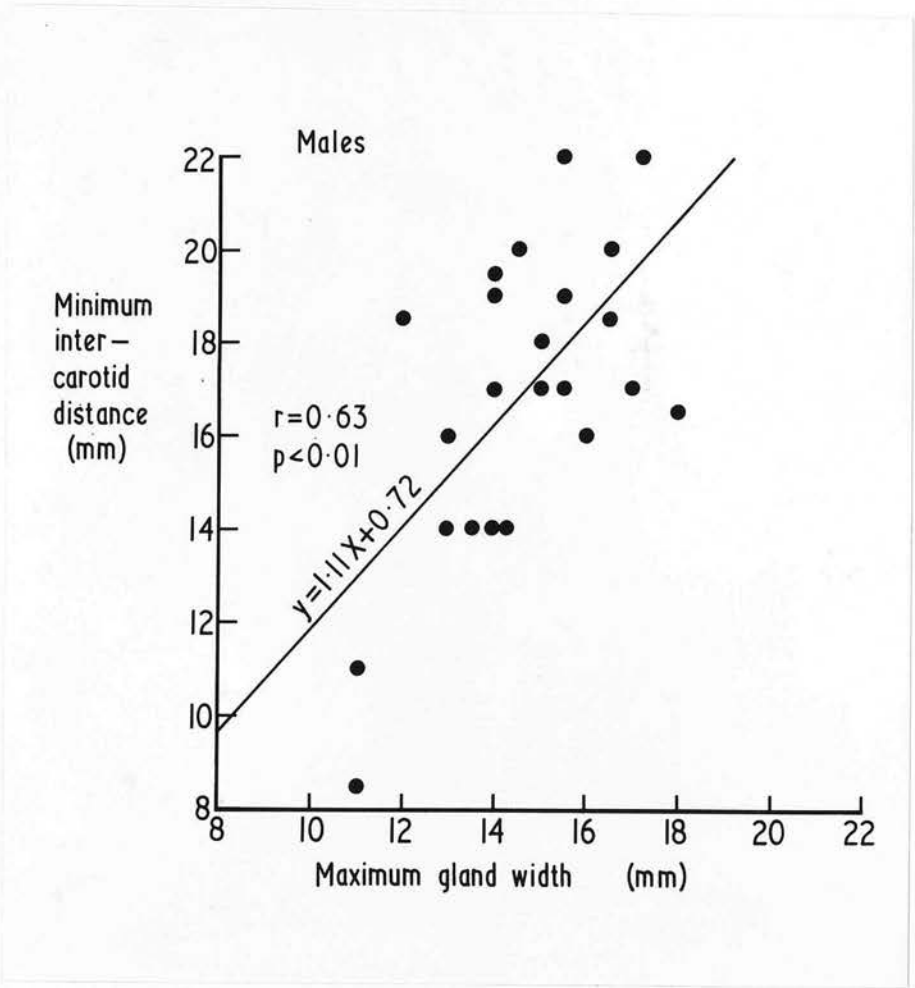

Figure 16

(a) Correlation of maximum gland width and minimum intercarotid distance (defined in text) for males. Minimum intercarotid distance varies from 8.5 to 22 mm (mean 17.0 mm). In 3 out of 23 males, maximum gland width exceeds minimum intercarotid distance.

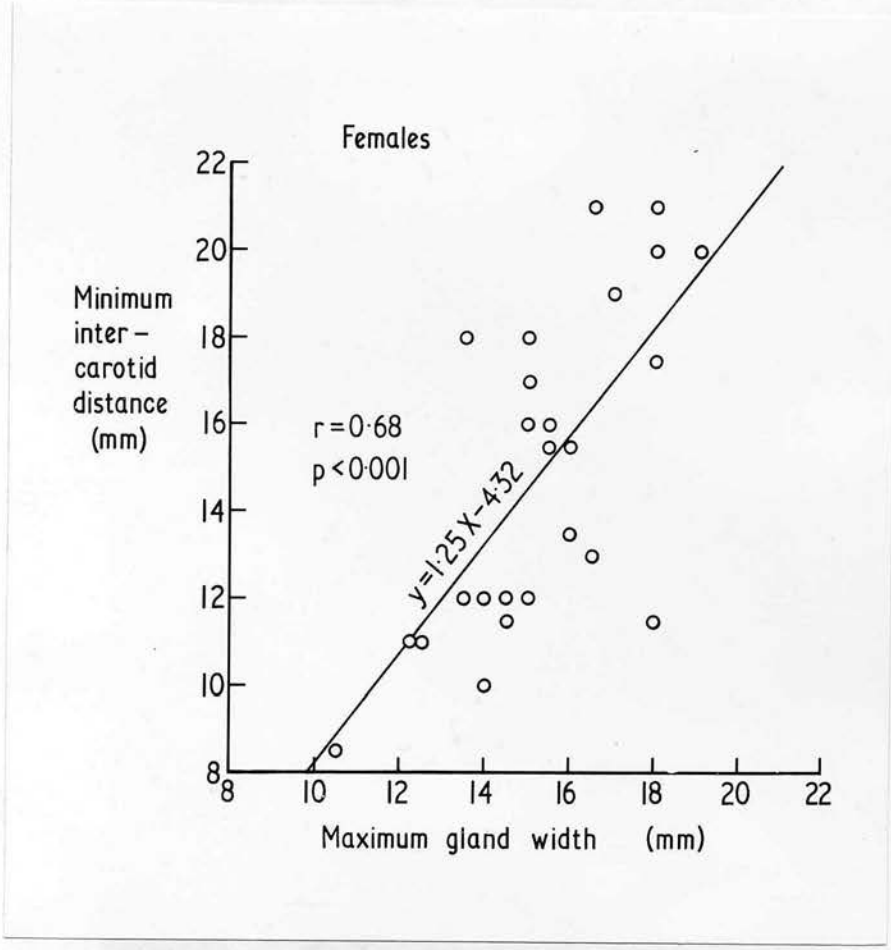

Figure 16 (cont.)

(b) Correlation of maximum gland width and minimum intercarotid distance for females. Minimum intercarotid distance varies from 8.5 to 21 mm (mean 14.9 mm). In 13 out of 25 females, maximum gland width exceeds minimum intercarotid distance.

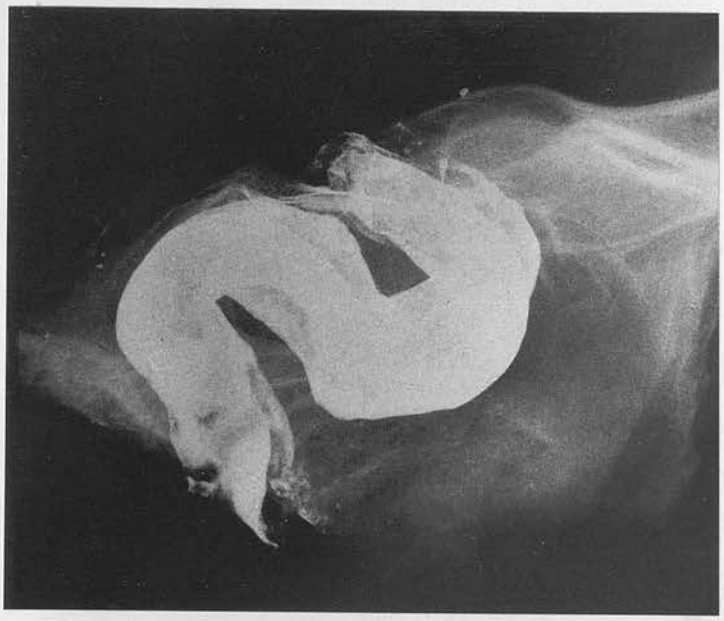

a

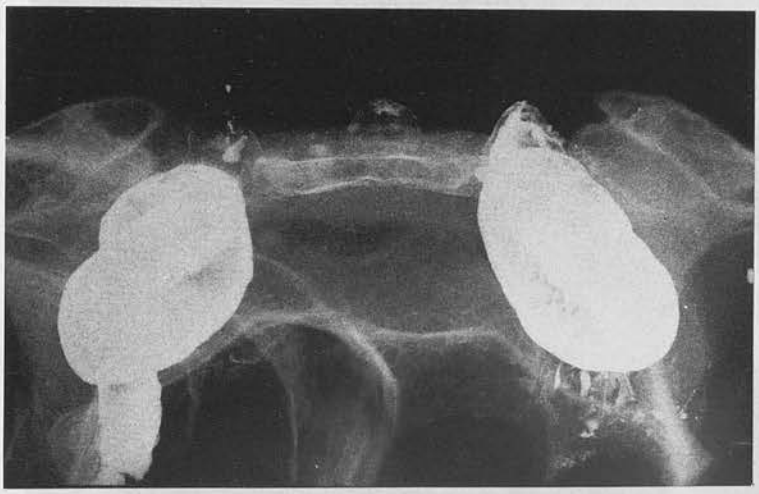

b

Figure 17

Lateral (a) and antero-posterior radiographs (b) of pituitary fossa. Tortuous carotid siphons may reach the upper half of the dorsum and undercut the posterior clinoids. (In this and all subsequent lateral radiographs of the sella in Part II anterior aspect lies to the right).

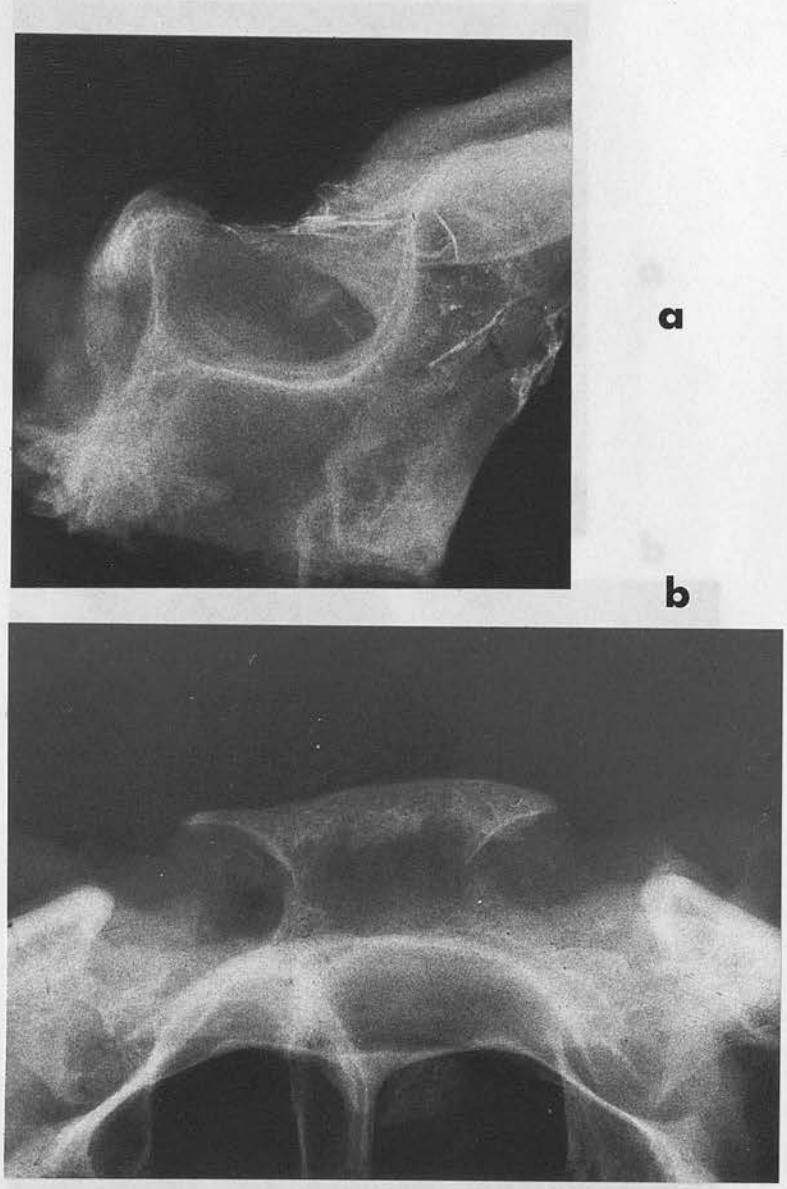

Figure 18

Lateral radiograph (a) of a fossa showing "thinning" of the dorsum, and antero-posterior radiograph (b) showing undercutting of the posterior clinoids. Petro-clinoid calcification is present. The diaphragma is outlined by bismuth in (a) and lies in normal position.

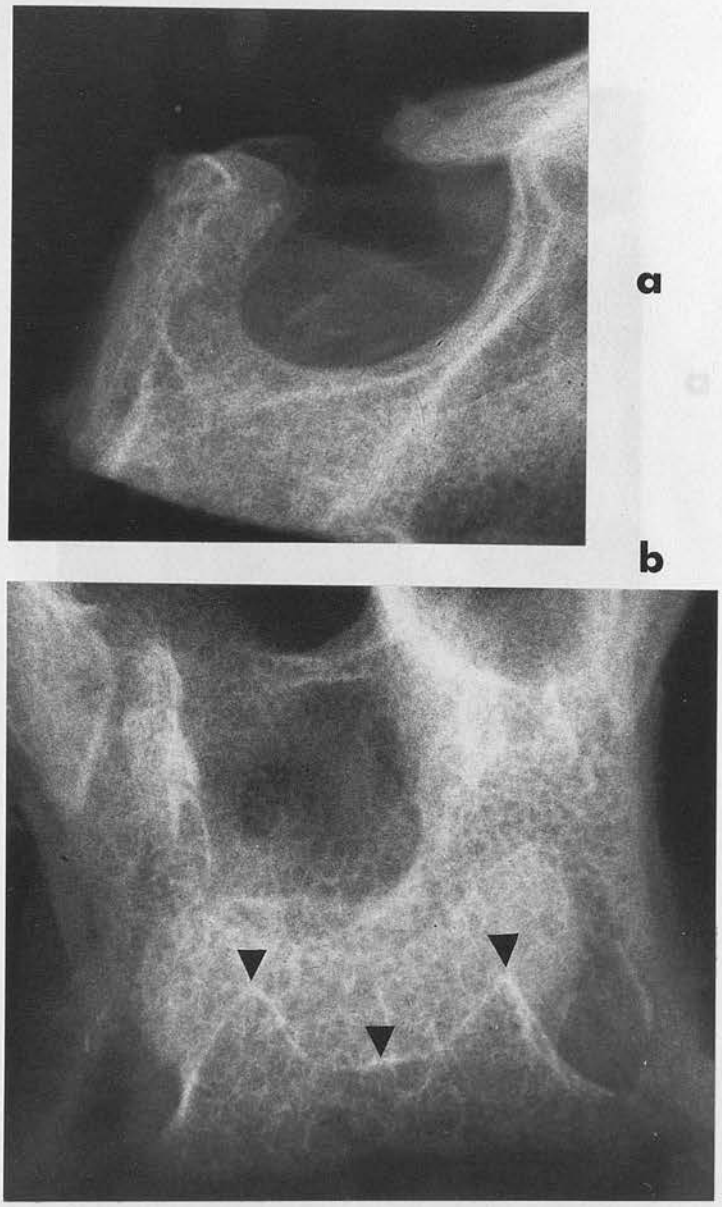

Figure 19

Configuration of a normal dorsum sellae. Lateral (a) and supero-inferior (b) radiographs showing how the apparent thickness of the dorsum in a lateral radiograph is due in part to the curve of the dorsum, which is arrowed in (b). Anterior aspect is uppermost in (b).

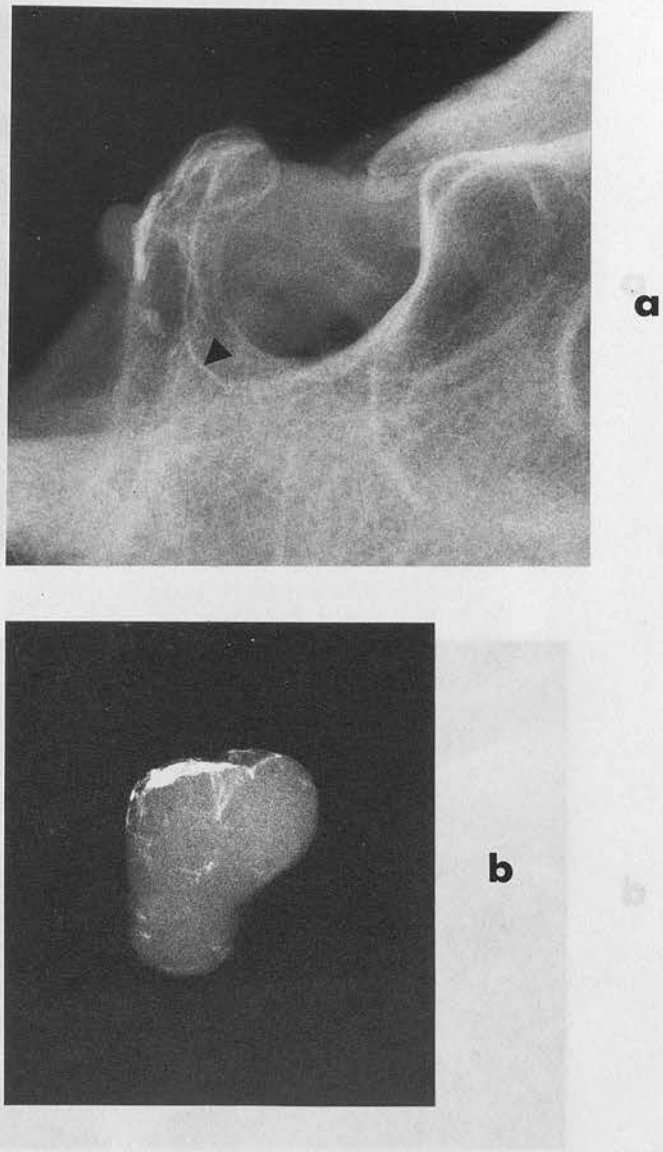

Figure 20

Lateral radiographs of the fossa (a) and gland (b). The recess in the lower part of the dorsum in (a) (arrowed) was occupied by a long postero-inferior projection of the pituitary gland. This recess has been called the "fossetta pituitaria". Bismuth powder is shown on the upper surface of the gland in (b).

a

b

Figure 21

The tuberculum sellae may be difficult to define.

(a) and (b) are examples of markedly different anterior configurations. The tuberculum sellae is arrowed in each case. In (a) the chiasmatic sulcus is the vertical step immediately above the tuberculum. In (b) the chiasmatic sulcus curves gently and the tuberculum is merely a tiny projection on this curve.

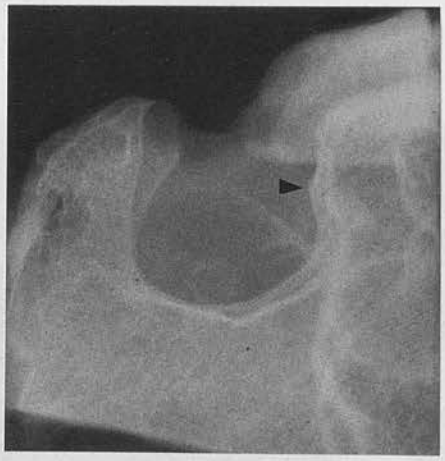

c

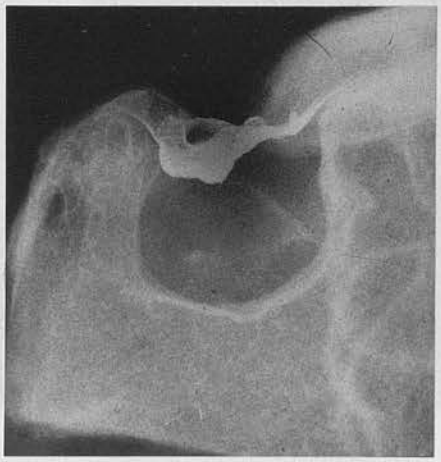

d

Figure 21 (cont.)

(c) and (d) are lateral radiographs of a fossa before and after outlining of the diaphragma with bismuth. A middle clinoid process is arrowed in (c). In (d) the diaphragma, which is slightly sunken in its central part, is shown attached to the tuberculum. This configuration could be confused with the one shown in (a).

Figure 22

Photograph of superior aspect of a fossa (anterior aspect uppermost) showing a middle clinoid process on the left (arrowed). The anterior and posterior clinoids are bridged and on the right, the middle clinoid is joined to this bridge to form the carotico-clinoid foramen, the centre of which is marked "O".

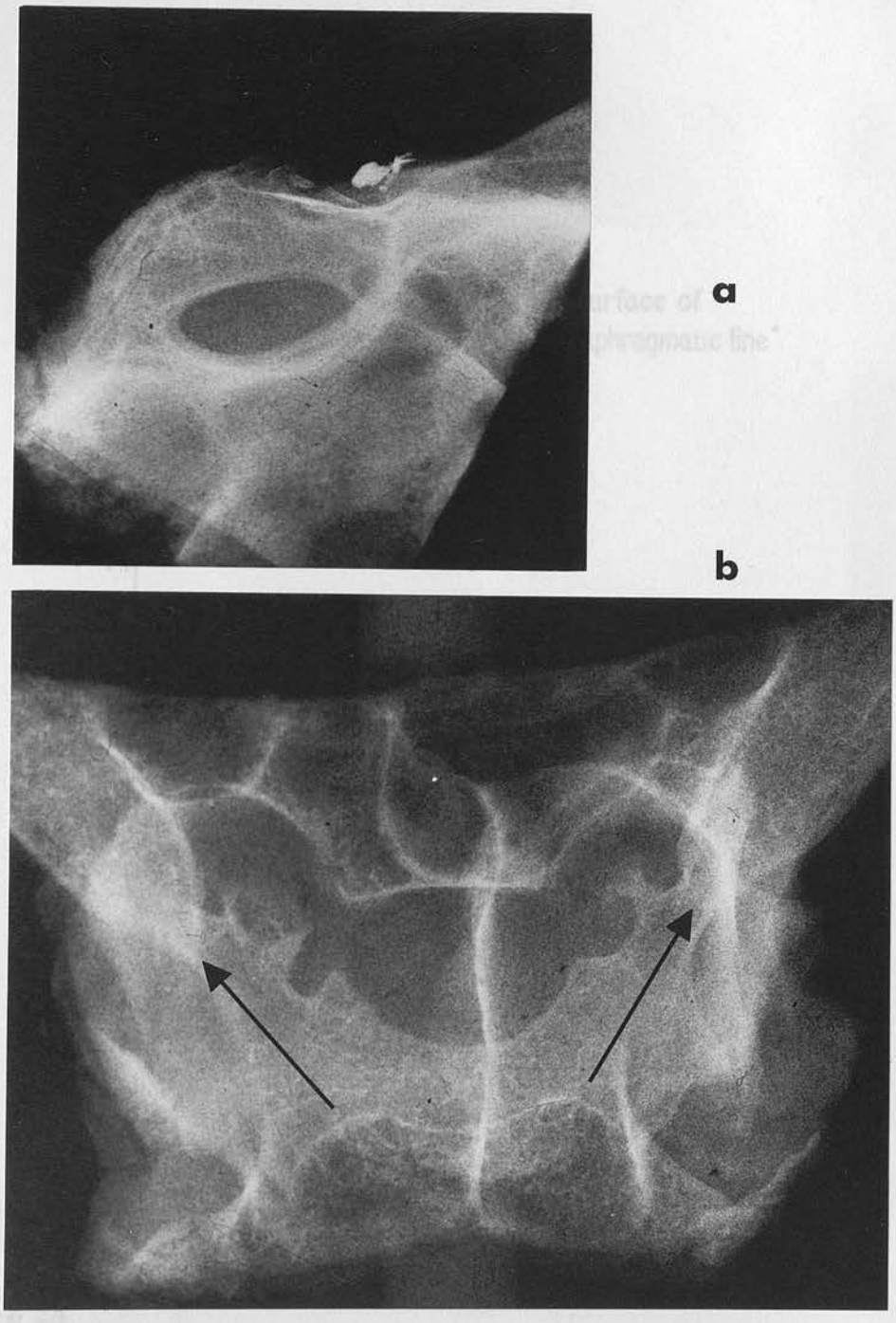

Figure 23

"Bridged" fossa. Lateral (a) and supero-inferior (b) radiographs. In (a) the diaphragma has been outlined and is in normal position. In (b) arrows lie along the bony bridges between anterior and posterior clinoids and point to the anterior clinoids.

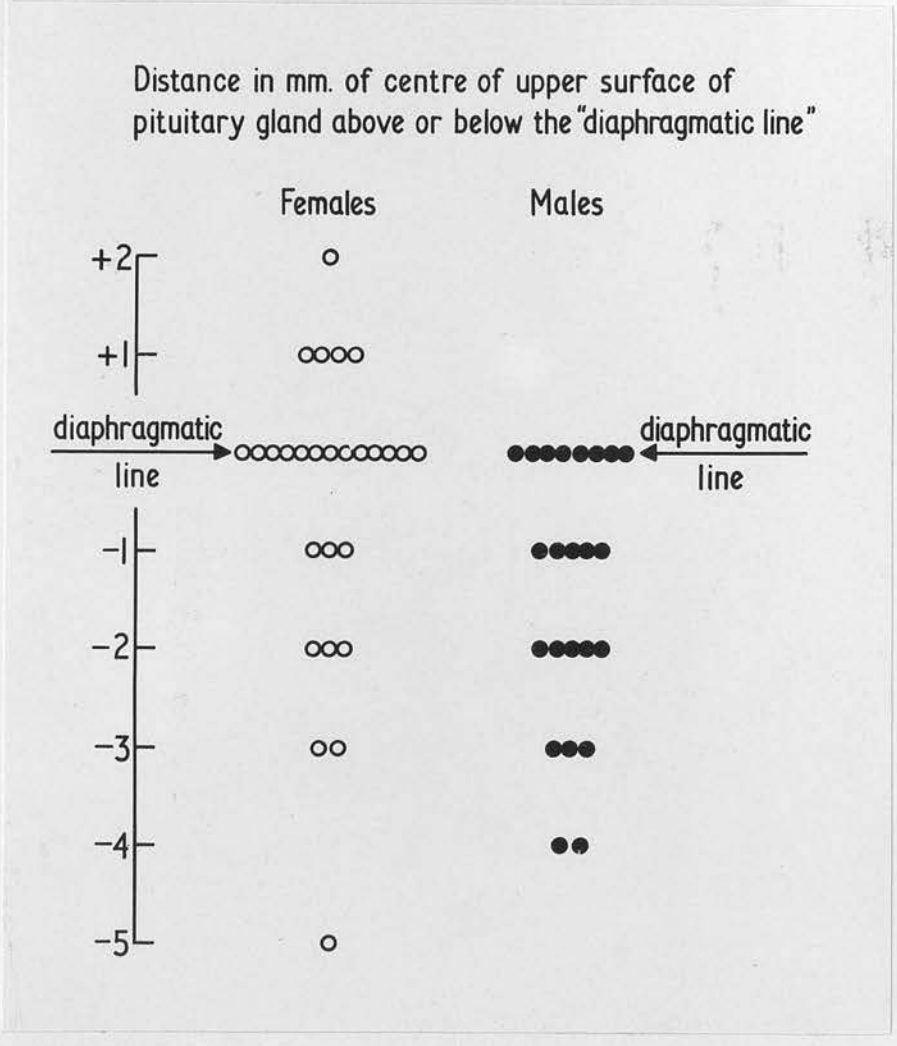

Figure 24

Variation in position of the centre of the upper surface of the gland above or below the "diaphragmatic line". The variation is greater in women. In 5 women the centre of the upper surface of the gland was above the "diaphragmatic line". The most markedly "sunken" gland was also found in a woman, illustrated in Fig. 25 (a) and (b).

a

b

Figure 25

Variations in contour of diaphragma.

(a) and (b) are lateral radiographs of the fossa and gland of a 79 year old woman. The diaphragma (outlined with bismuth), is markedly sunken, as is the upper surface of the gland, the centre of which lies 5 mm below the "diaphragmatic line".

c

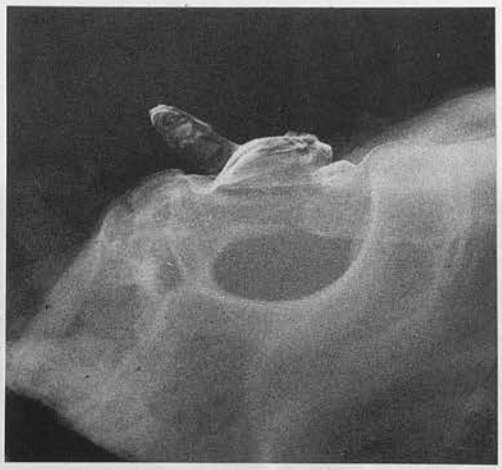

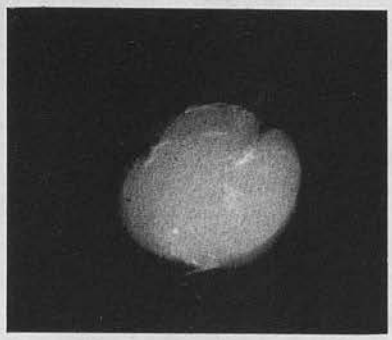

d

Figure 25 (cont.)

(c) and (d) are lateral radiographs of the fossa and gland of a 22 year old female. The diaphragma is pushed upwards by a bulky gland which was otherwise normal. The centre of the diaphragma lies 2 mm above the "diaphragmatic line".

Figure 26

Fenestrated diaphragma (not from consecutive series).

(a) Photograph of the diaphragma from above. The upper arrows lie on the optic nerves, the lower arrow on the pituitary stalk. The web-like diaphragma is clearly shown.

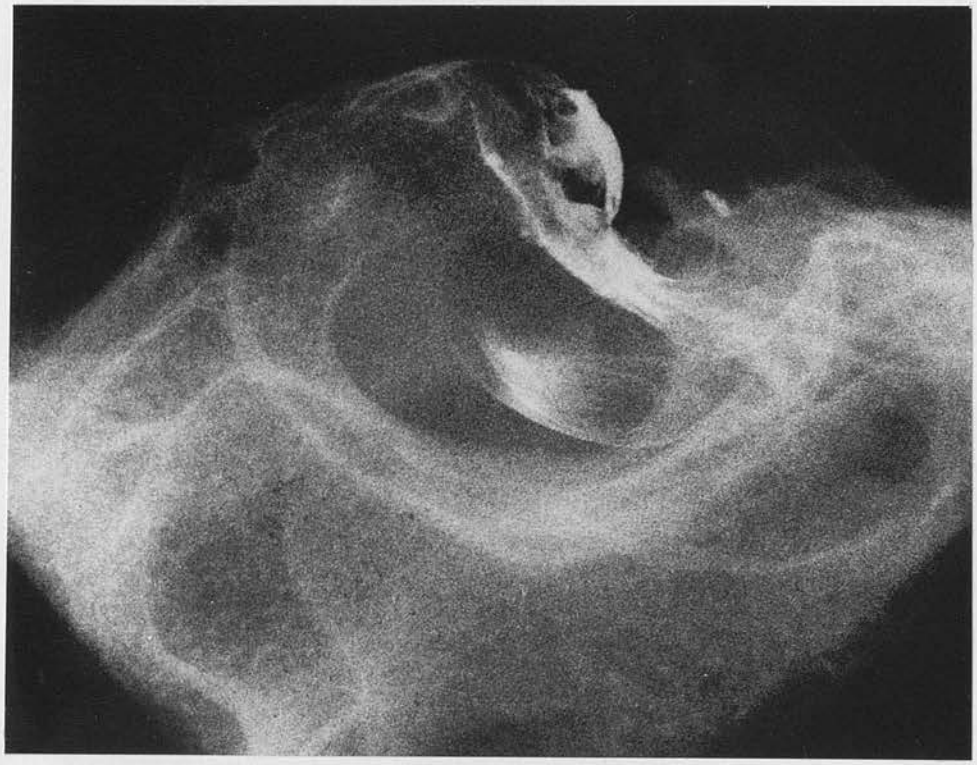

Figure 26 (cont.)

(b) Lateral radiograph of the same case. The diaphragma and part of the upper surface of the gland are outlined with bismuth. The upper surface of the gland is well below the diaphragma.

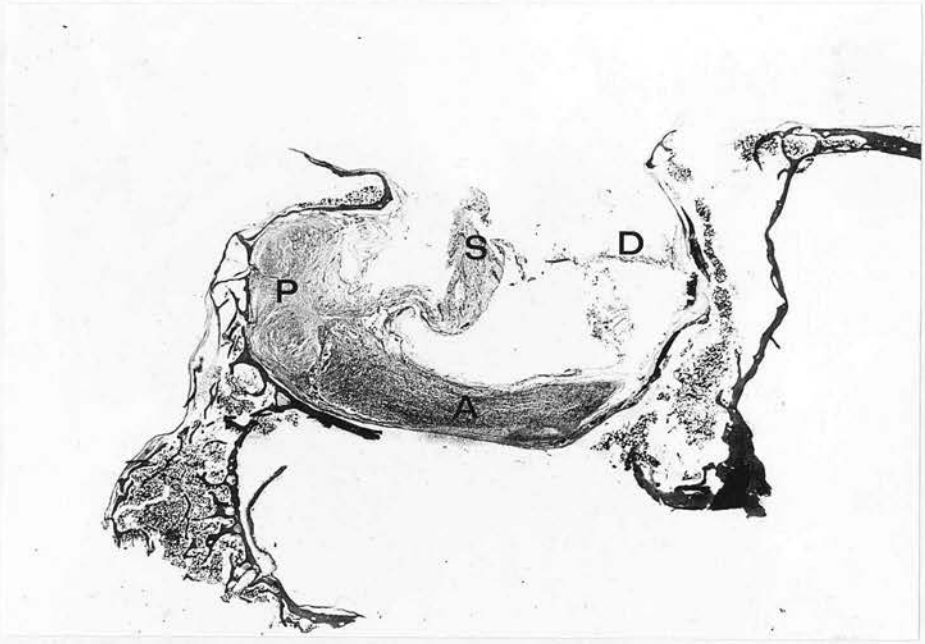

Figure 26 (cont.)

(c) Decalcified sagittal section of the fossa and gland. Despite the extreme central depression of the gland, it was histologically normal. It formed a layer spread over the floor and lateral walls of the fossa (H & E x 4.5).

A = anterior lobe; P = posterior lobe; S = stalk; D = diaphragma.

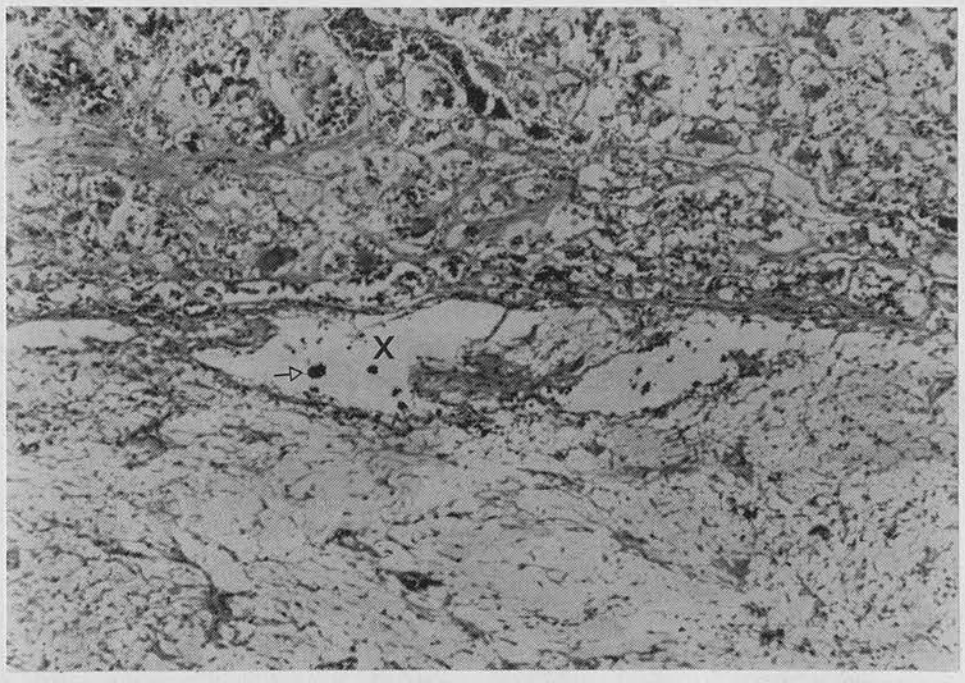

Figure 27

Horizontal section through the pituitary gland of a male of 68 years. Note the central cavity (x) containing black bismuth particles (one is arrowed) which lies between the anterior lobe (above) and the posterior lobe (below). This cavity was shown on serial section to be a tubular structure in communication with the subarachnoid space (H & E x 70).

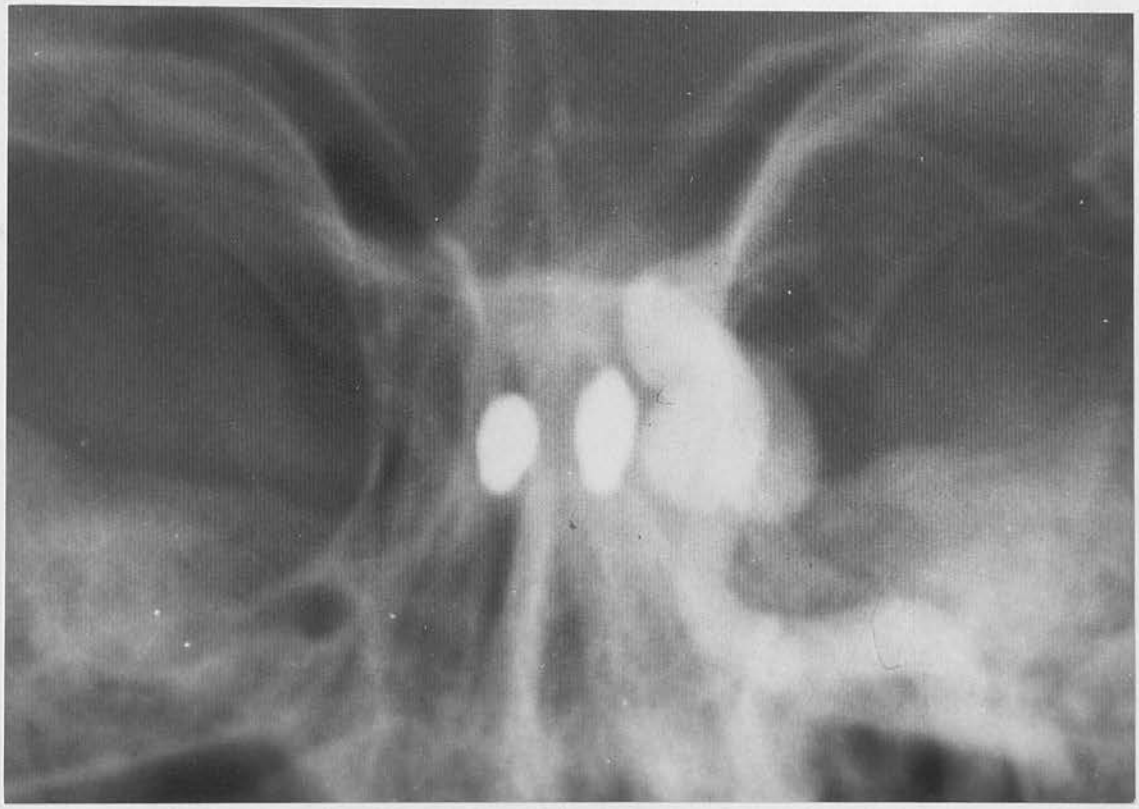

Figure 28

Left carotid arteriogram a few days after a technically satisfactory pituitary implant in which modified Forrest screws were used. The patient, suffering from metastatic breast cancer, subsequently died from a subarachnoid haemorrhage. The left screw is within 1 mm of a previously undeclared aneurysm of the carotid siphon.

PART III

ASSESSMENT OF RADIOLOGICAL CRITERIA OF SELLAR ABNORMALITY ON PLAIN FILMS AND TOMOGRAPHY

Figures 29 - 43

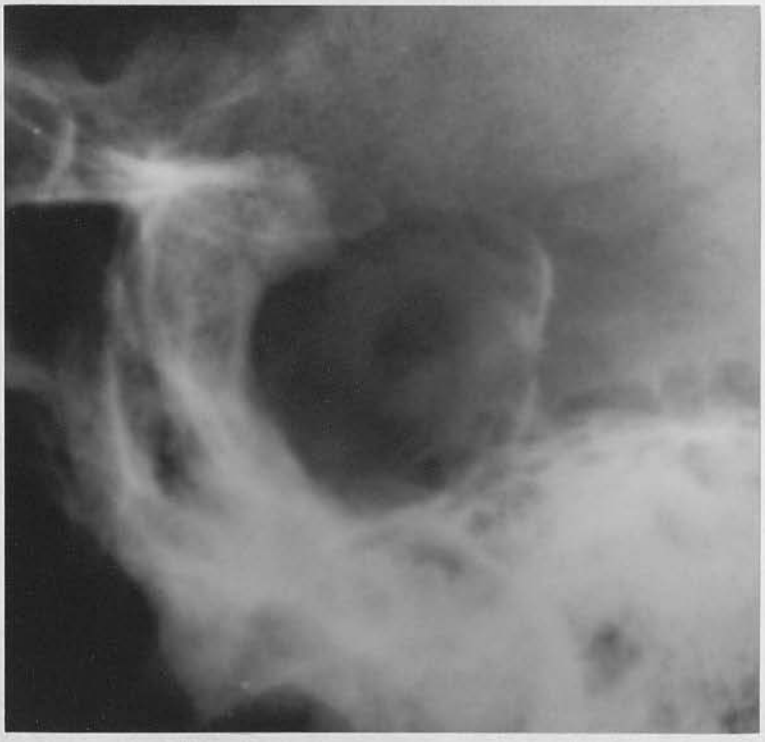

Figure 29

Example of Group A fossa. Marked sellar enlargement, with erosion of the bony outline. (In this and all subsequent lateral films of the fossa in Part III the anterior aspect lies to the left).

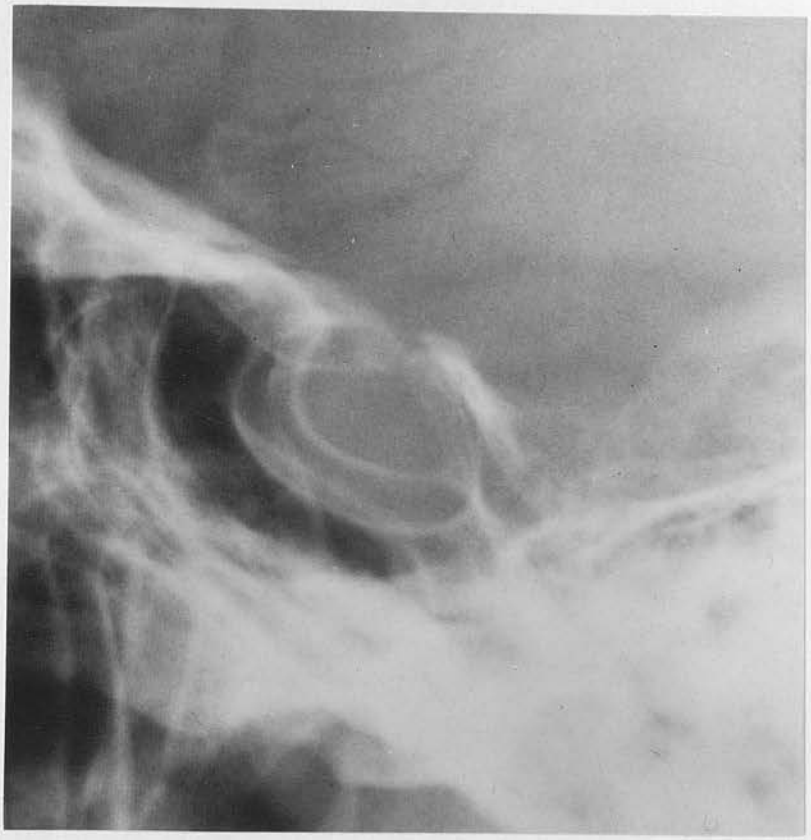

Figure 30

Example of Group B fossa. Well marked double contour, the inner one being intact. Petro-clinoid calcification.

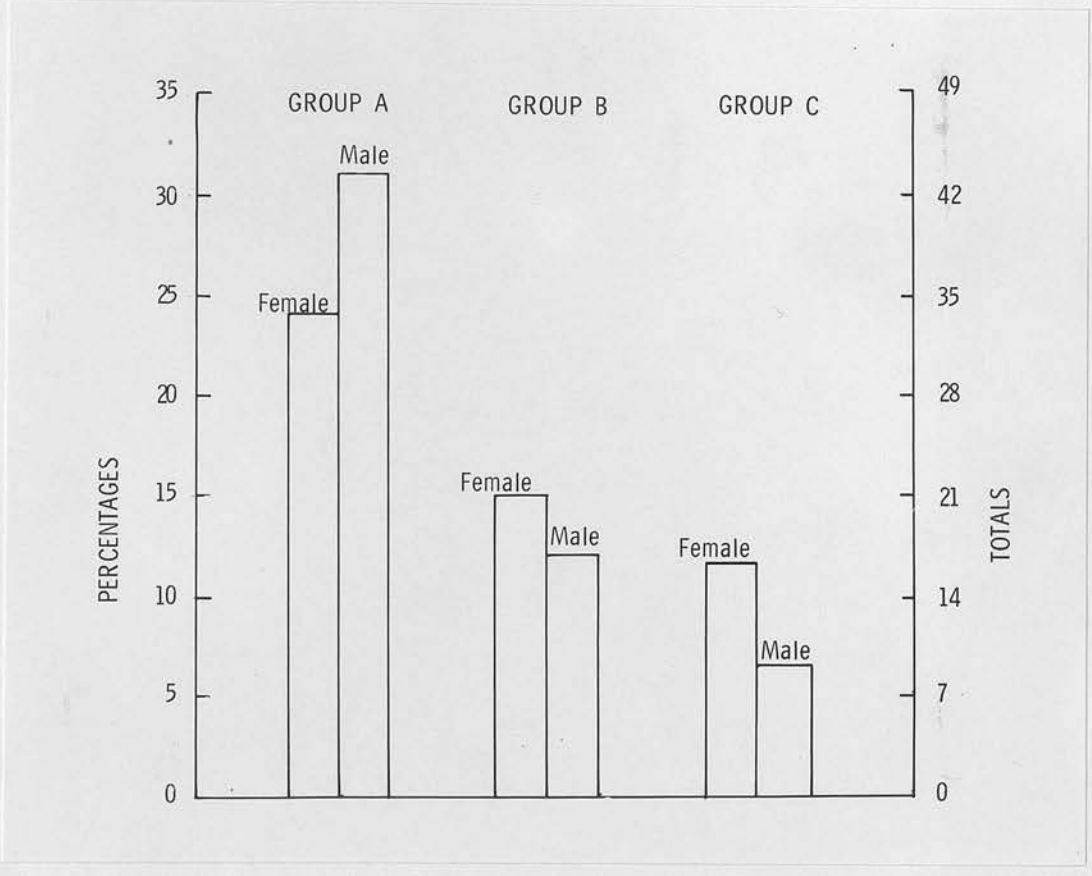

Figure 31

Numbers and percentages of acromegalic patients in Groups A, B and C, sexes shown separately.

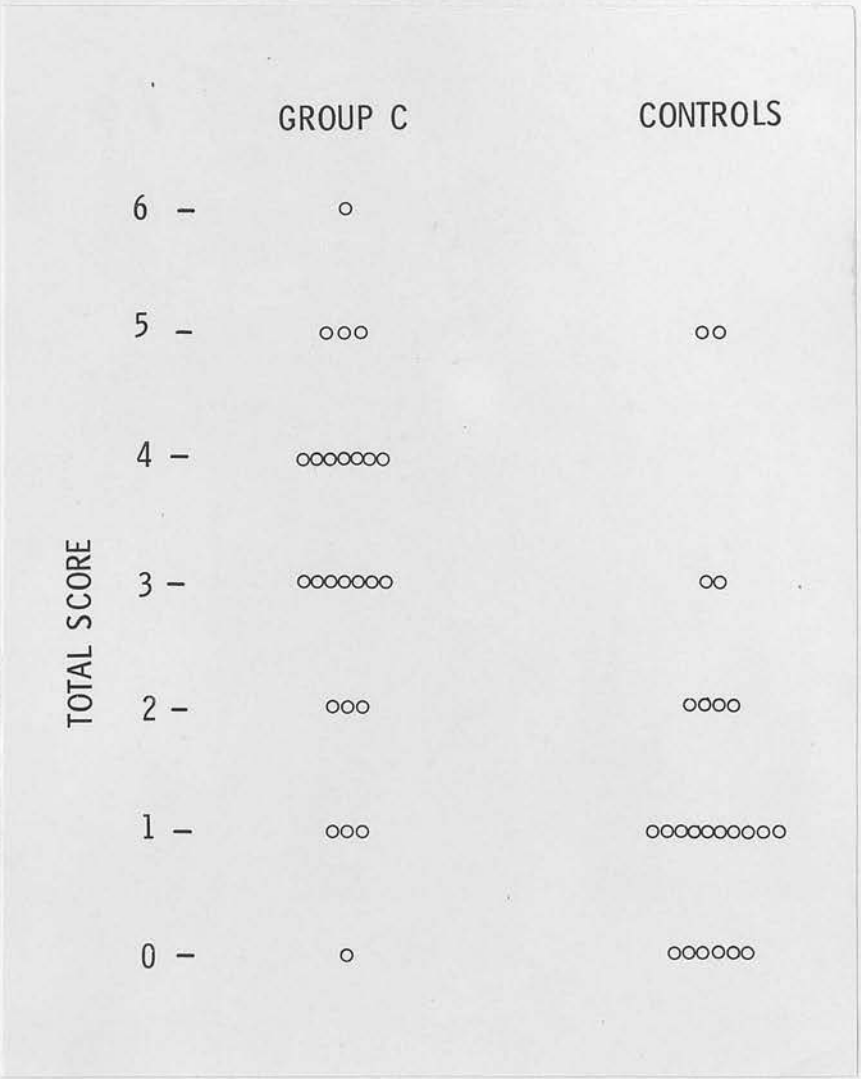

Figure 32

Total scores for plain film analysis in Group C acromegalic fossae and controls. Each circle represents one patient. If the two control fossae with a score of five are considered to be abnormal (see text), the normal range is represented by scores of 0 to 3.

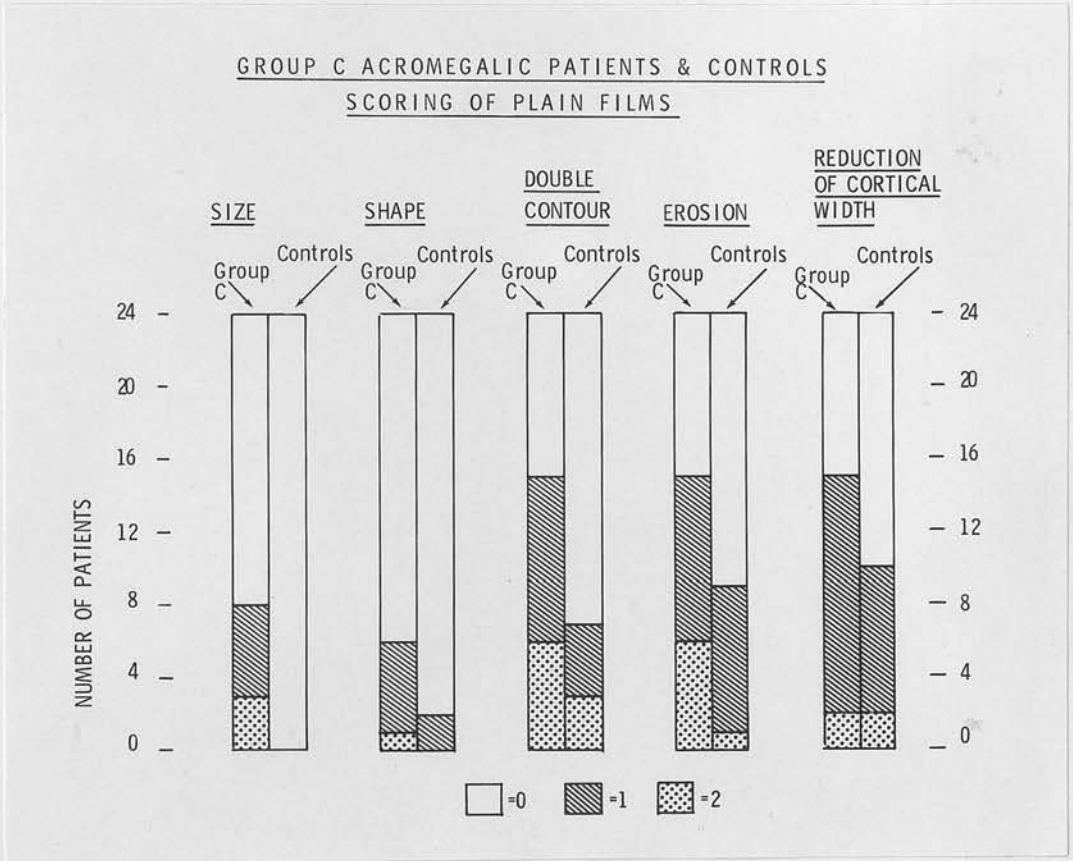

Figure 33

Plain film scores in Group C fossae and controls. Each of the five features compared. For each feature, a score of 0, 1 or 2 indicates that it was judged to be within normal limits, doubtful or abnormal respectively.

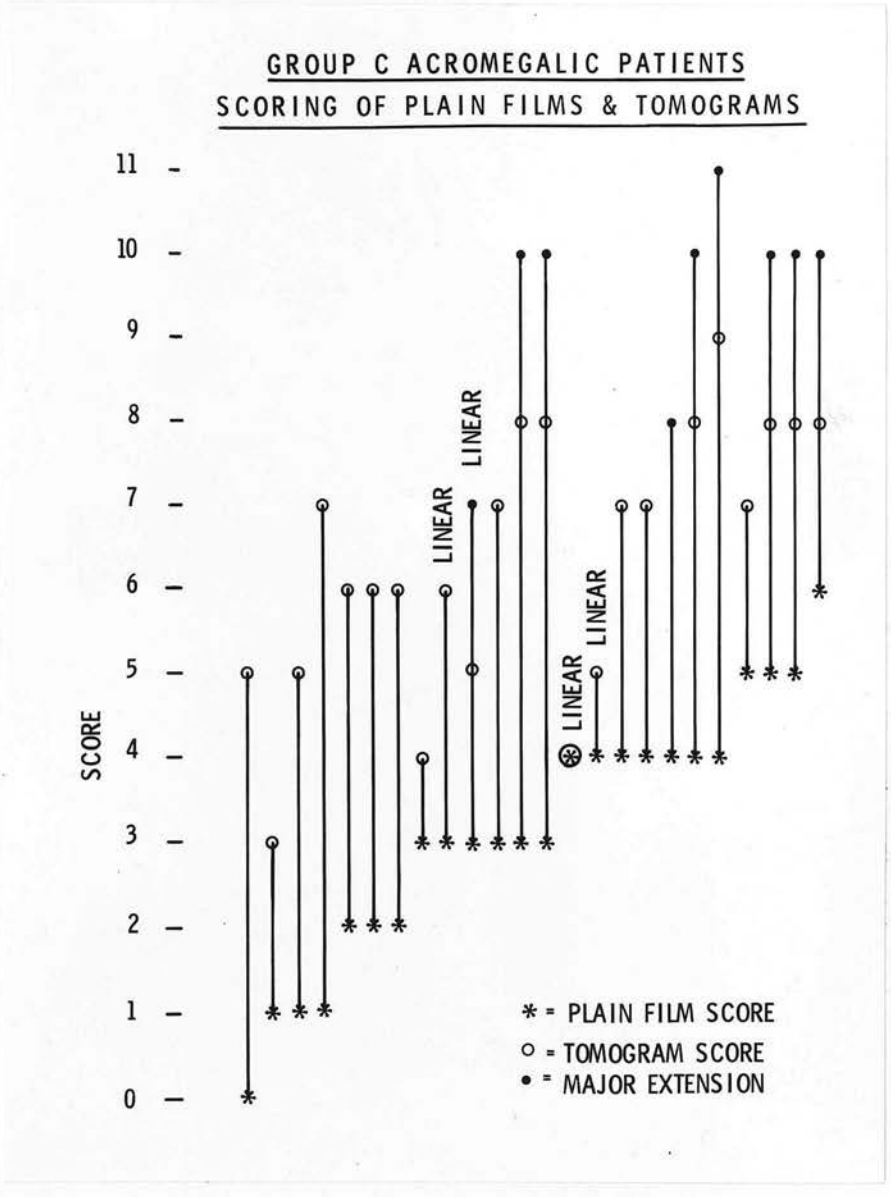

Figure 34

Comparison of total scores for plain films and tomography in Group C. A major downward extension of tumour (for which two points were added to the tomogram score) was shown in nine patients. Tomography was hypocycloidal in all except four (labelled).

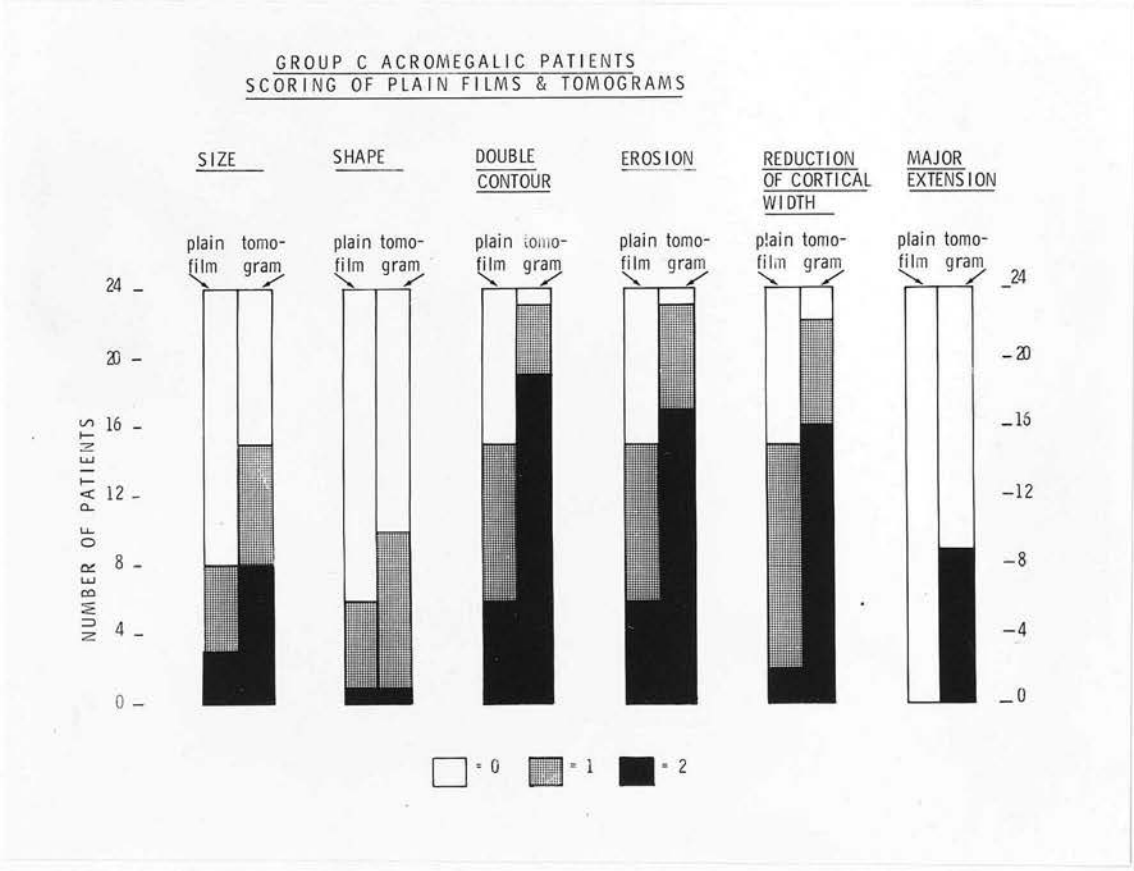

Figure 35

Comparison of plain film and tomogram scores in Group C. For each feature, separately assessed, a score of 0, 1 or 2 means within normal limits, doubtful or abnormal respectively.

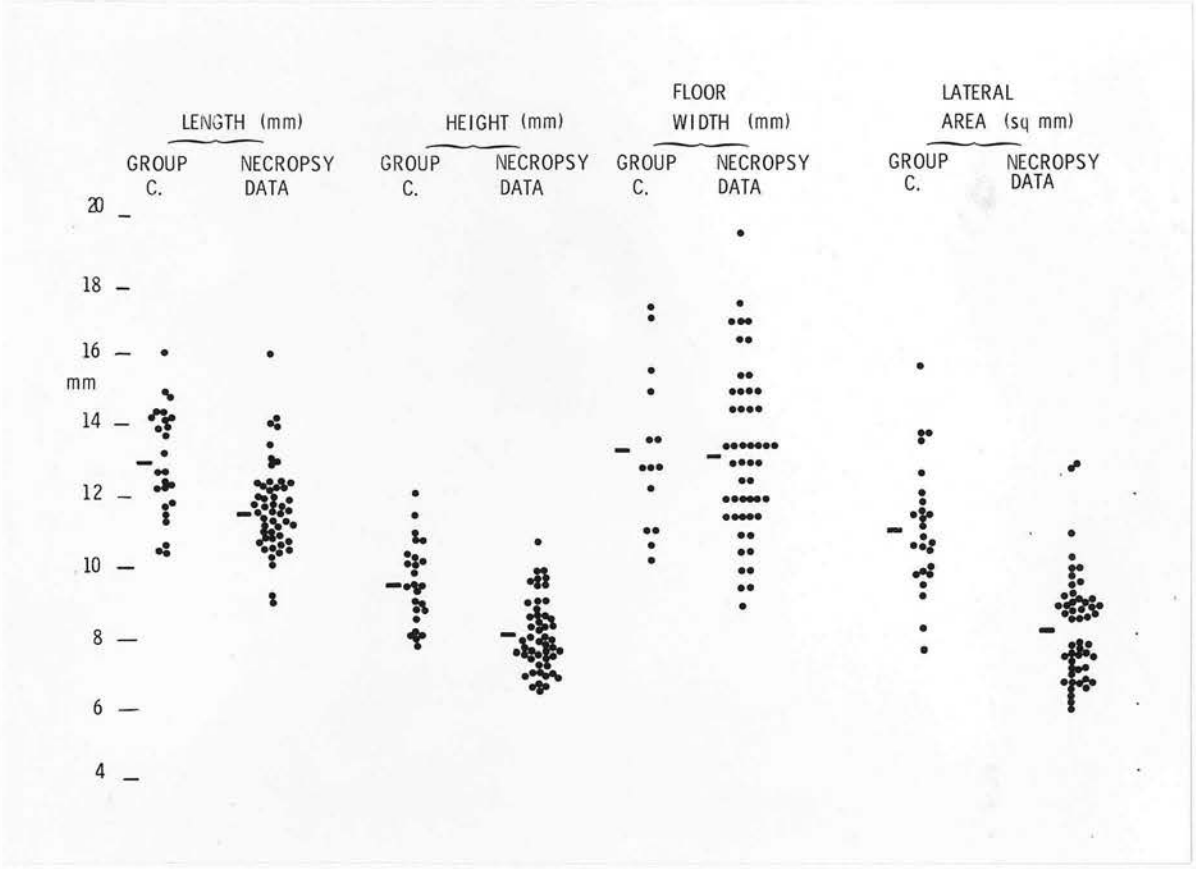

Figure 36

Sellar measurements in Group C and necropsy fossae compared. No Group C fossa showed increased length or width. Lateral area was increased in four, height in five. The floor was visible on postero-anterior films in only 14 fossae in Group C. The horizontal lines denote the means in each group.

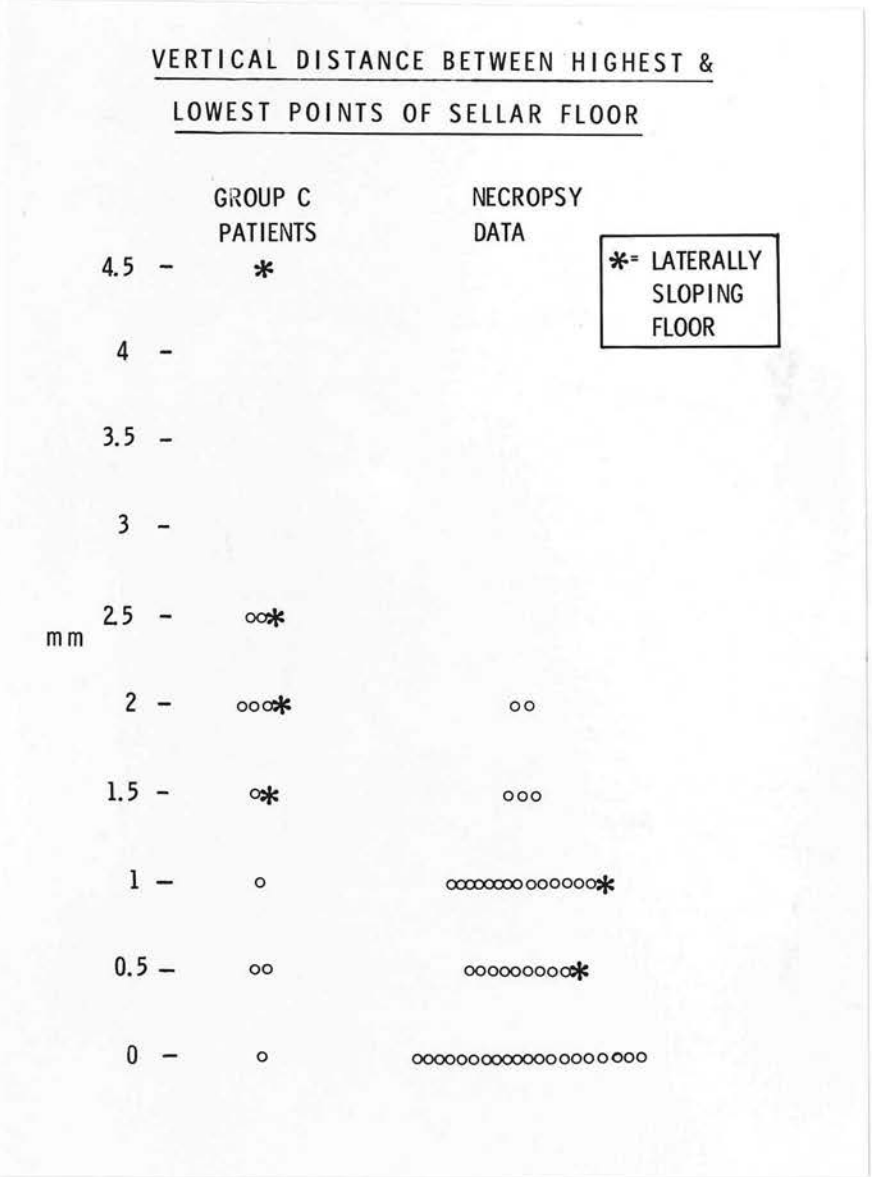

Figure 37

Central and lateral depression of the sellar floor measured on frontal films. Comparison with necropsy data. Central depression exceeded the normal range in only two Group C fossae. Lateral depression occurred less commonly in both groups but was greater in Group C than in necropsy fossae.

GROUP C PATIENTS

COMPARISON OF PLAIN FILM SCORES

AND BLIND ASSESSMENTS (RATED AS SHOWN)

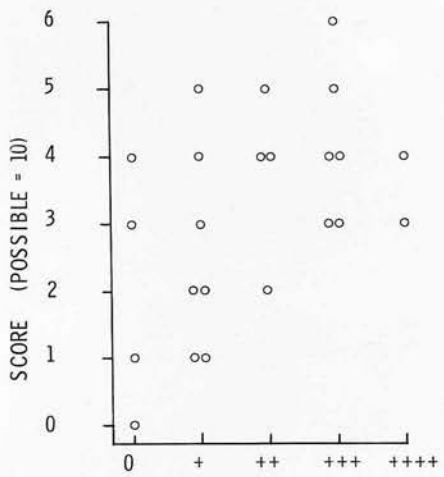

BLIND ASSESSMENT	RATING
2 NORMAL	0
1 NORMAL, 1 DOUBTFUL	+
2 DOUBTFUL* OR 1 NORMAL, 1 ABNORMAL†	++
1 DOUBTFUL, 1 ABNORMAL	+++
2 ABNORMAL	++++

Figure 38

Plain film scores for the fossae of Group C patients are compared with "blind" assessments of these fossae. Twelve Group C fossae were called normal by at least one "blind" observer.

(* three patients; † one patient).

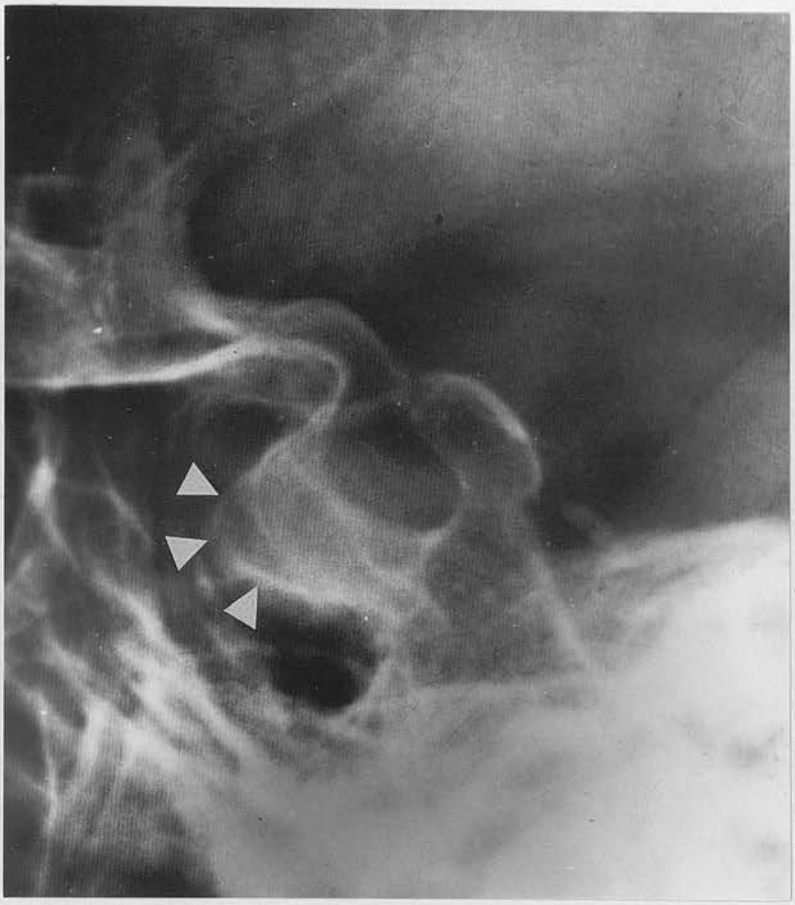

Figure 39

Example from Group B called normal by both "blind" observers. The intact inner contour distracts attention from the second outline (arrowed).

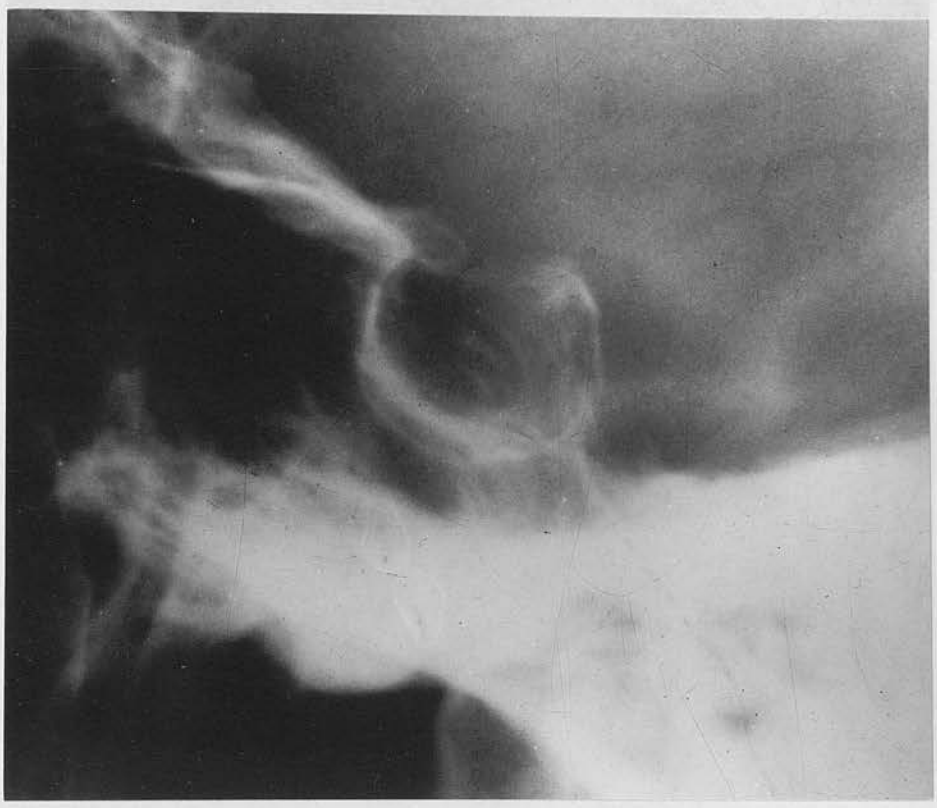

Figure 40

"Control" fossa. 51 year old, male diabetic. Plain film score of five. Double contour which is judged to be pathological. Carotid siphon calcification partially obscures detail and appearances were originally called normal on routine reporting.

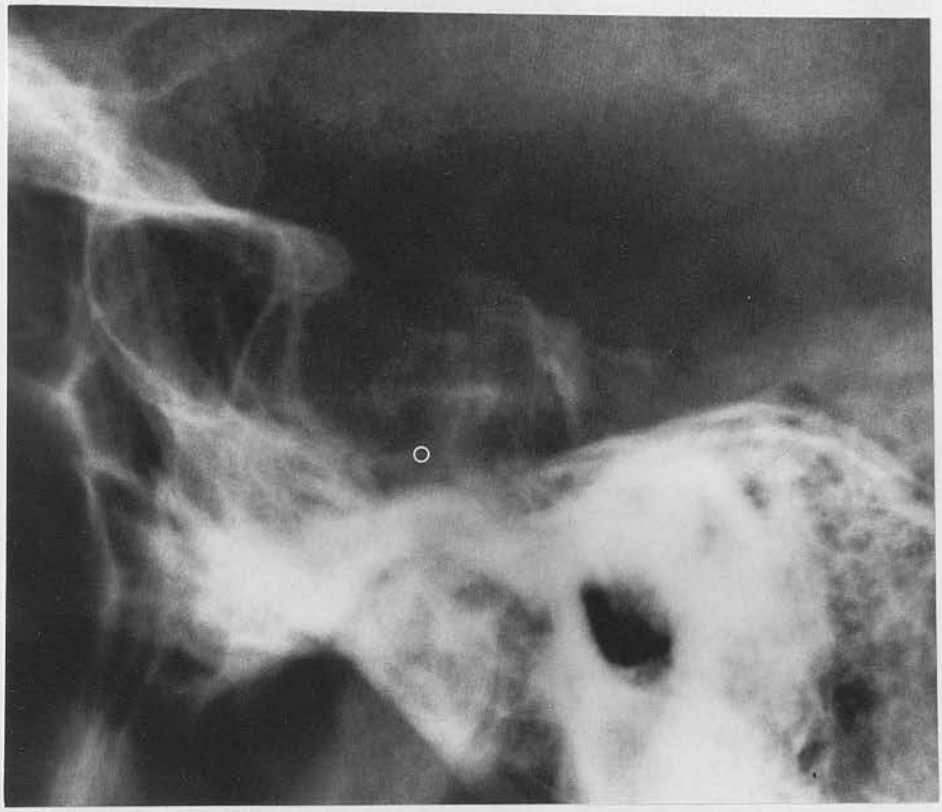

Figure 41

(a) Group A fossa showing enlargement and bone destruction. Petro-clinoid calcification.

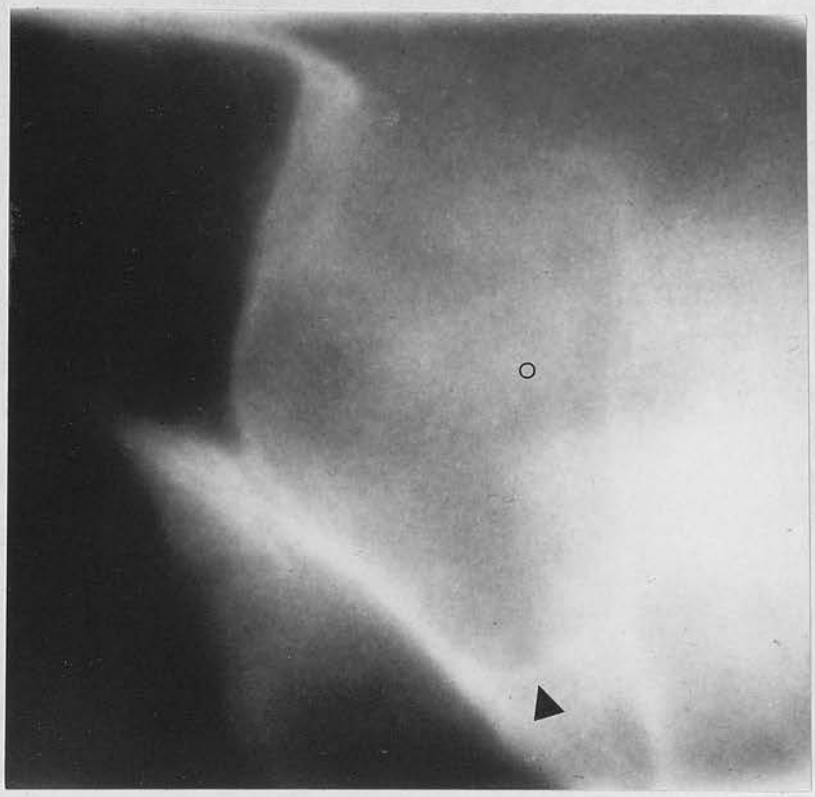

Figure 41 (cont.)

(b) Lateral tomography reveals the extent of downward extension (arrowed) concealed on plain films by overlying temporal bone.

The open circles lie at approximately the same anatomical level in (a) and (b).

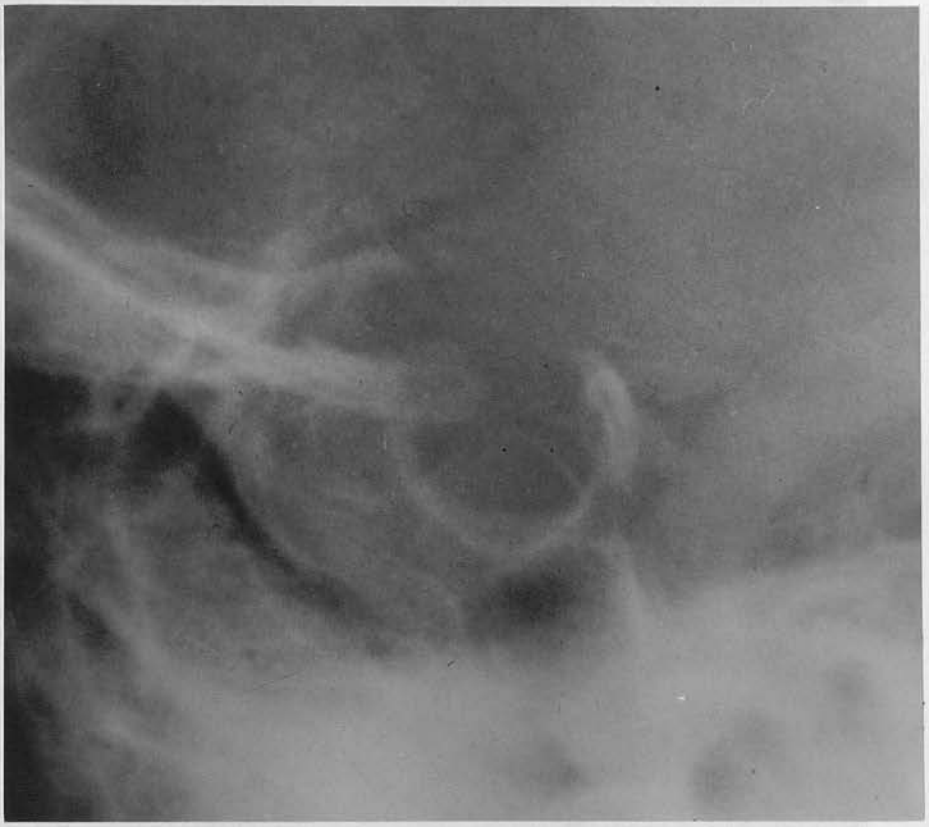

Figure 42

Group B fossa.

(a) A second contour is seen anteriorly.

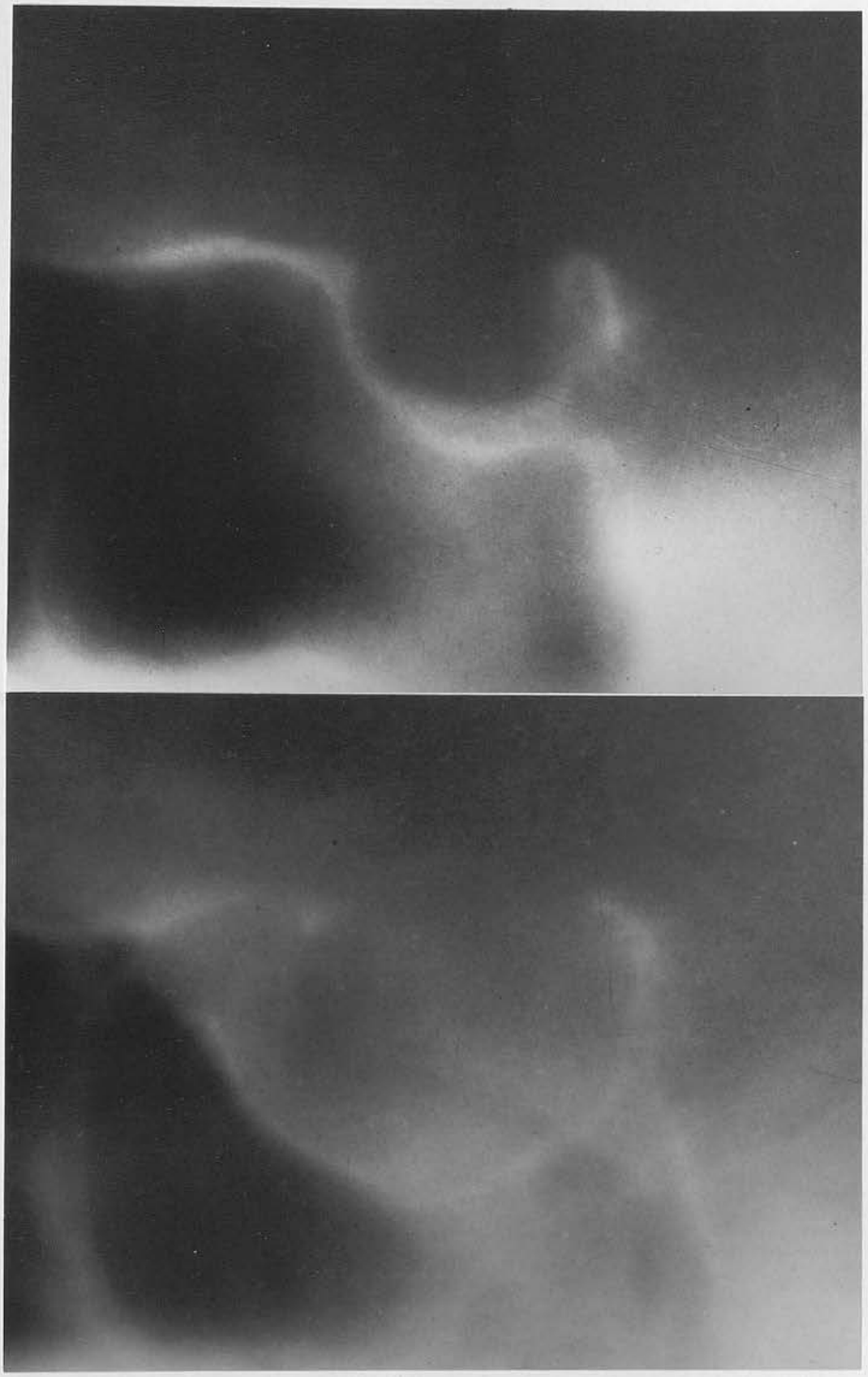

Figure 42 (cont.)

(b) and (c). Same patient as in (a). Lateral tomography shows the marked eccentricity of sellar enlargement. Tomography in a coronal plane is equally valuable in this situation.

Figure 43

(a) Group C fossa. Apparently normal sellar dimensions. Plain film score of five.

Figure 43 (cont.)

(b) Same patient as in (a). Lateral tomography shows a large extension into the sphenoid sinus, totally unexpected from the plain films. Tomogram score of ten.

PART IV

DEMONSTRATION OF PARASELLAR ANATOMY BY PNEUMOENCEPHALOGRAPHY COMBINED WITH TOMOGRAPHY

Figures 44 - 52

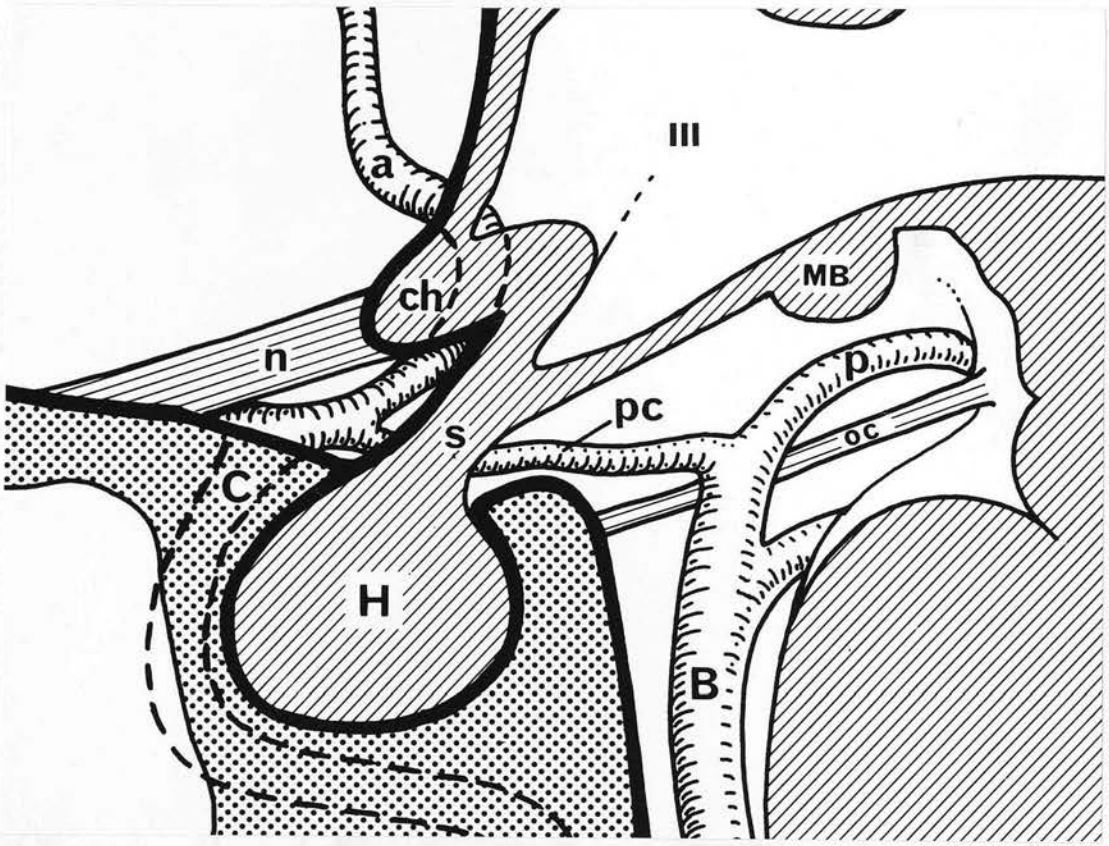

Figure 44

(a) Parasellar anatomy in the sagittal plane, shown diagramatically. Anterior aspect lies to the left as it does in all subsequent illustrations in the sagittal plane in Part IV.

III = third ventricle; H and S = pituitary gland and stalk respectively; ch and n = optic chiasm and nerve respectively; MB = mamillary body; oc = oculomotor nerve; C = carotid artery; a = anterior cerebral artery; p = posterior cerebral artery; pc = posterior communicating artery; B = basilar artery.

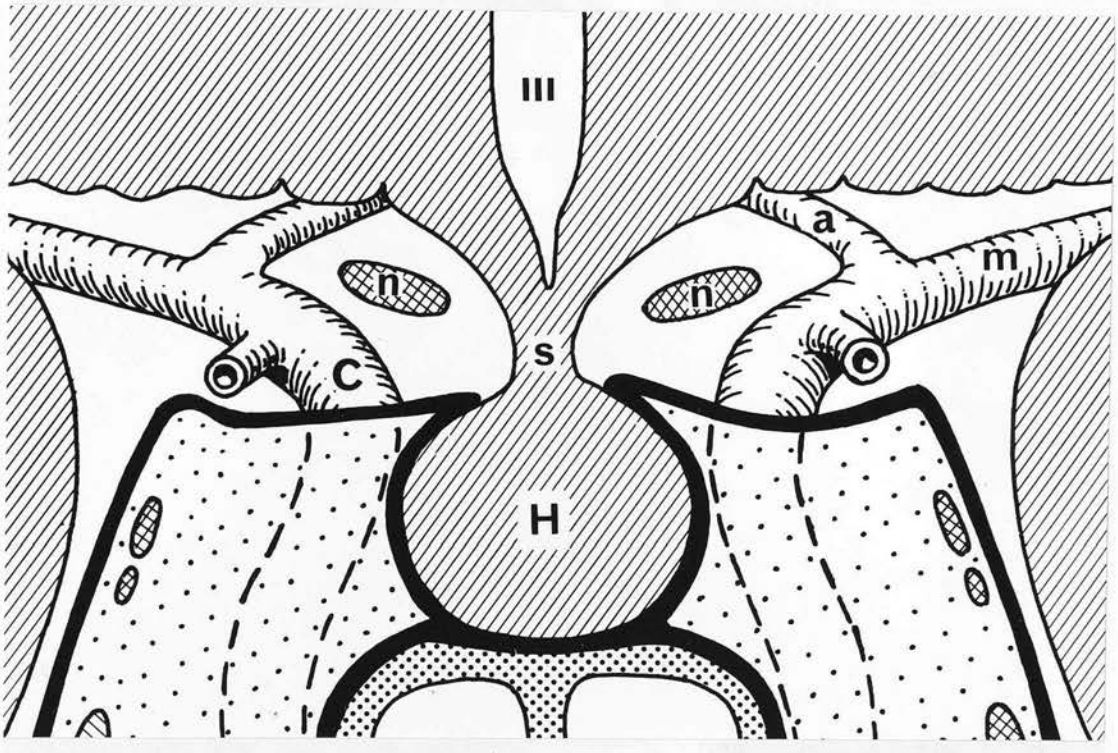

Figure 44 (cont.)

(b) Parasellar anatomy in the coronal plane, shown diagramatically.

III = third ventricle; H and S = pituitary gland and stalk respectively; n = optic nerves; C = carotid artery; m = middle cerebral artery.

Figure 45

Position for tomography in the sagittal plane. A harness supports the head which rests on a foam-rubber pad. Introduction of gas usually requires a temporary change in position. The table is later placed horizontal for tomography in the coronal plane.

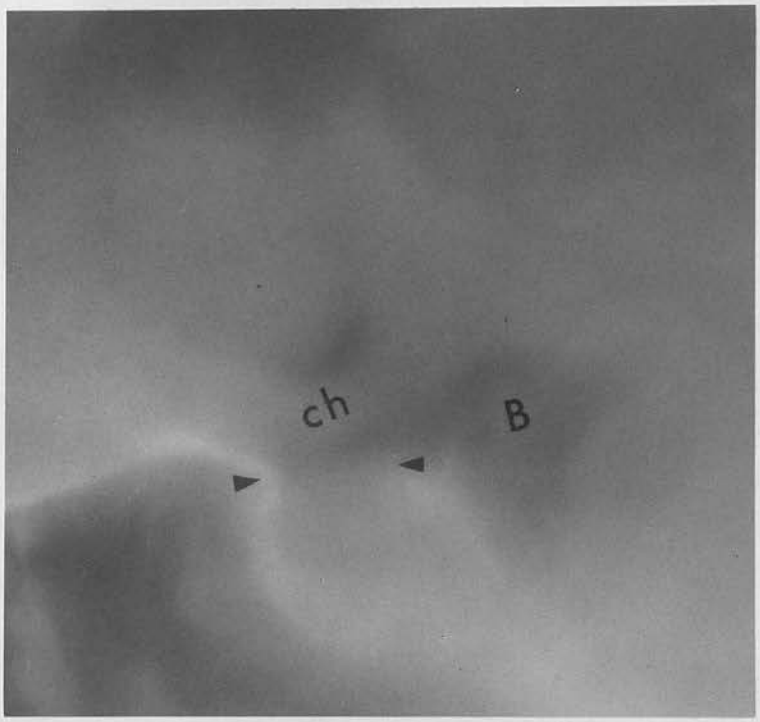

Figure 46

(a) Acromegalic patient (D. B.). Normal suprasellar anatomy. Sagittal plane. Pneumoencephalogram with circular tomography. The diaphragma sellae runs between the arrowheads marking the tuberculum and the most anterior point of the convexity of the tip of the dorsum. Optic chiasm (ch) and basilar artery (B) are labelled.

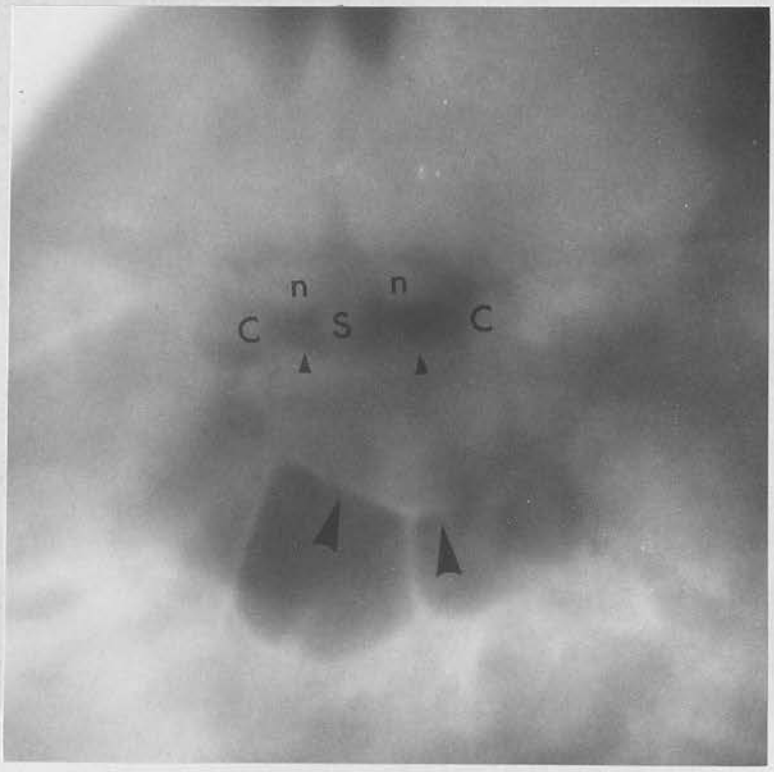

Figure 46 (cont.)

(b) Same patient (D. B.). Normal suprasellar anatomy. Coronal plane. Pneumoencephalogram with circular tomography. Small arrowheads mark the diaphragma. Pituitary stalk (S) and optic nerves (n), individually demonstrated, are well seen. The supraclinoid portions of the carotid siphons (C) are also shown. Large arrowheads mark the partly destroyed sellar floor.

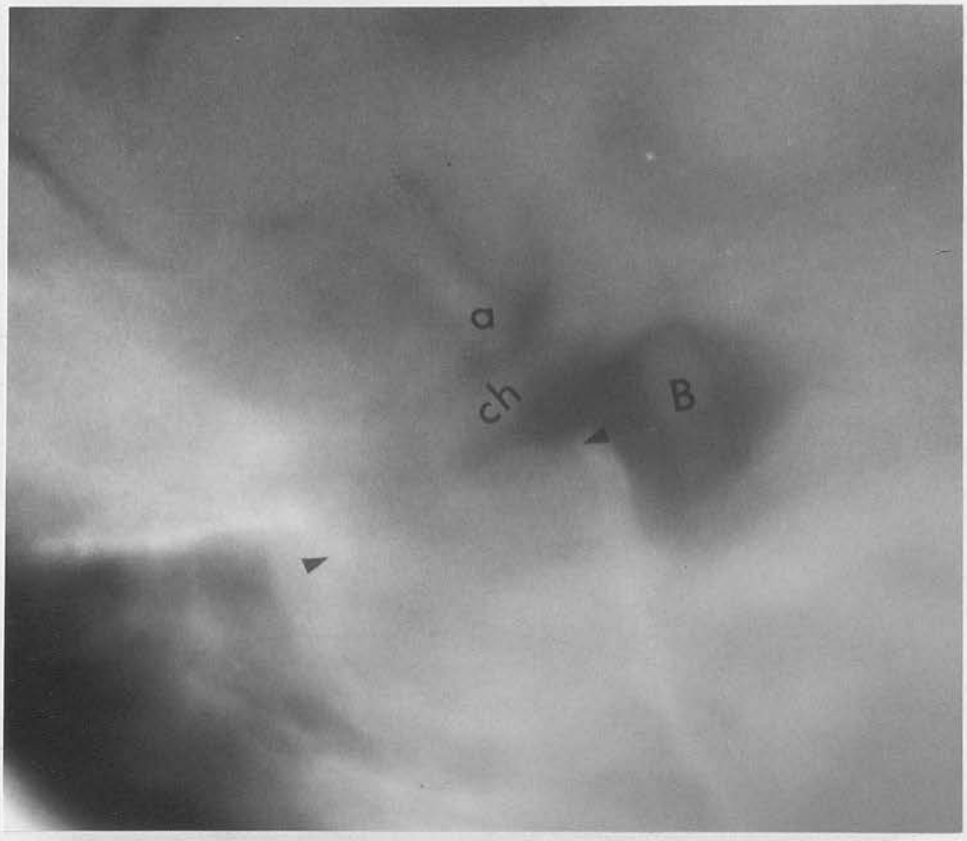

Figure 47

Acromegalic patient (D. H.). Normal suprasellar anatomy. Sagittal plane. Arrowheads mark the anterior convexity of the tip of the dorsum and the tuberculum. Optic chiasm is labelled (ch). Immediately posterior to it lies the pituitary stalk (unmarked). Basilar (B) and anterior cerebral arteries (a) are also indicated. In this instance only the posterior half of the diaphragma has been outlined. In 14 out of 20 patients with normal suprasellar anatomy the entire upper surface of the diaphragma was shown.

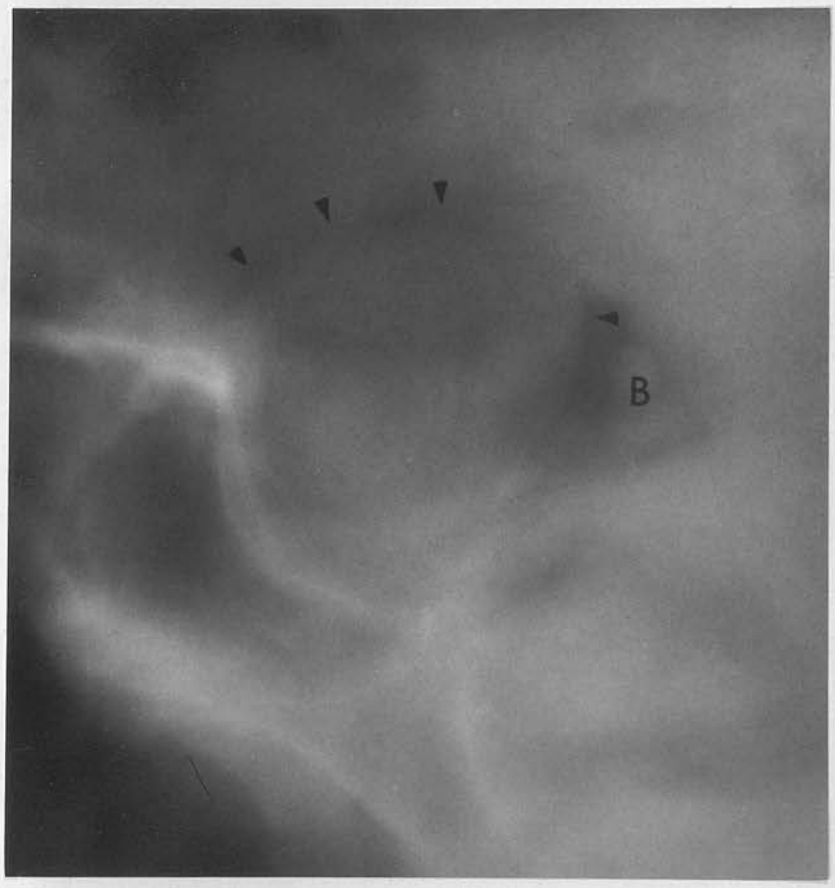

Figure 48

(a) Patient with chromophobe adenoma (A. Z.). Moderate suprasellar extension (defined in text). Sagittal plane. Visual deterioration for previous four months. The upward extension (arrowed) is well shown, including its anterior aspect. Of ten moderate or large suprasellar extensions (see text) the anterior aspect was delineated in eight. Basilar artery is also seen (B).

Figure 48 (cont.)

(b) Same patient (A. Z.). Coronal plane. Carotid arteries (C) are shown closely related to the lateral aspects of the suprasellar tumour, which is arrowed. Sellar floor is marked by a single large arrowhead.

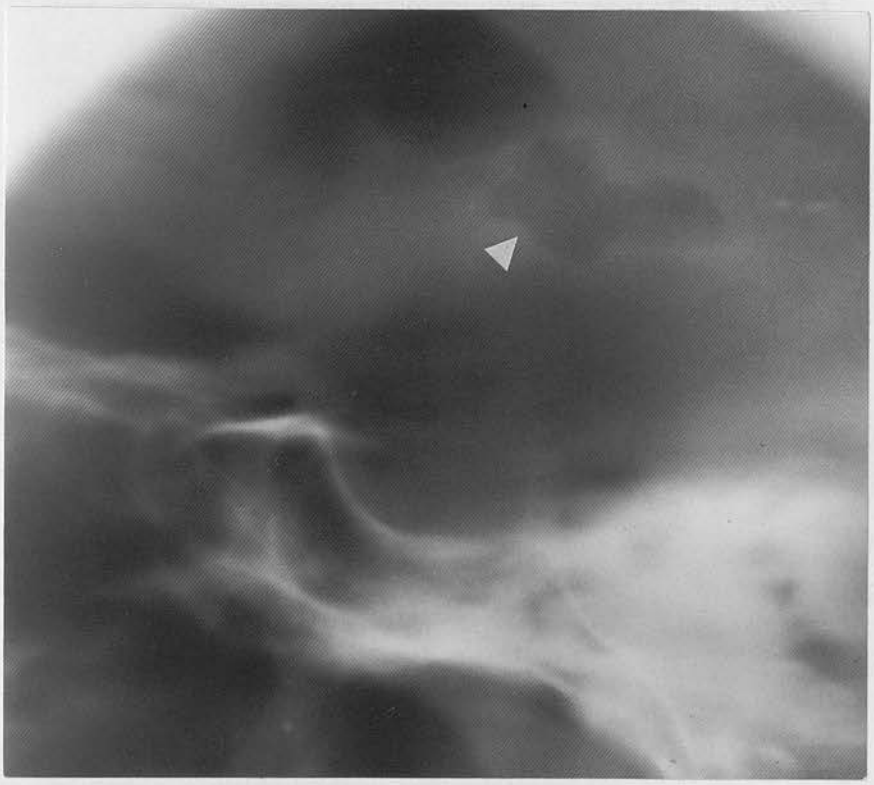

Figure 48 (cont.)

(c) Same patient (A. Z.). Hanging head autotomogram showing indentation of the anterior end of the third ventricle (arrowed) by the tumour. Though large or moderate suprasellar extensions always deformed the anterior end of the third ventricle, hanging head autotomography did not provide a detailed demonstration of the tumour itself. Small suprasellar tumours did not declare themselves in this way.

Figure 49

(a) Acromegalic patient (D. Ba.). Moderate suprasellar extension. Sagittal plane. Normal visual fields which deteriorated rapidly after pituitary implant. The upward extension (arrowed) and the pituitary stalk (S) are well seen. The structure lying between the upper two arrowheads is probably right anterior cerebral artery, seen again in (b).

Figure 49 (cont.)

(b) Same patient (D. Ba.). Coronal plane. The transverse arrows lie on anterior clinoids. Large arrowheads mark the roof of the nasal cavity. The fossa floor is destroyed at this level and air in the sphenoid sinus gives a false impression of intrasellar gas. The right anterior cerebral artery (a) is also indicated.

Figure 49 (cont.)

(c) Same patient (D. Ba.). Hanging head autotomogram. The anterior end of third ventricle, though deformed, is obscured by collections of gas situated laterally.

Figure 50

(a) Patient with Chiari-Frommel syndrome (D. Be.). Sagittal plane. Large suprasellar extension (arrowed). Patient had left central scotoma and right temporal hemianopia.

Figure 50 (cont.)

(b) Same patient (D. Be.) ten months after pituitary implant of rods of Y-90. Sagittal plane. The suprasellar extension (arrowed) is much smaller. Full recovery of visual fields.

Figure 51

(a) Acromegalic patient (R. W.). Sagittal plane. Superior aspect of gland in normal position (arrowed). Diabetic retinopathy was also present and pituitary implant aimed at pituitary ablation.

Figure 51 (cont.)

(b) Same patient (R. W.), eight months after pituitary implant of Y-90. Sagittal plane. Intrasellar gas is shown, the pituitary gland being shrunken within the sella. The fine line running between the arrowheads is interpreted as the diaphragma outlined by gas above and below. Optic chiasm (ch) and anterior cerebral artery (a) are also shown.

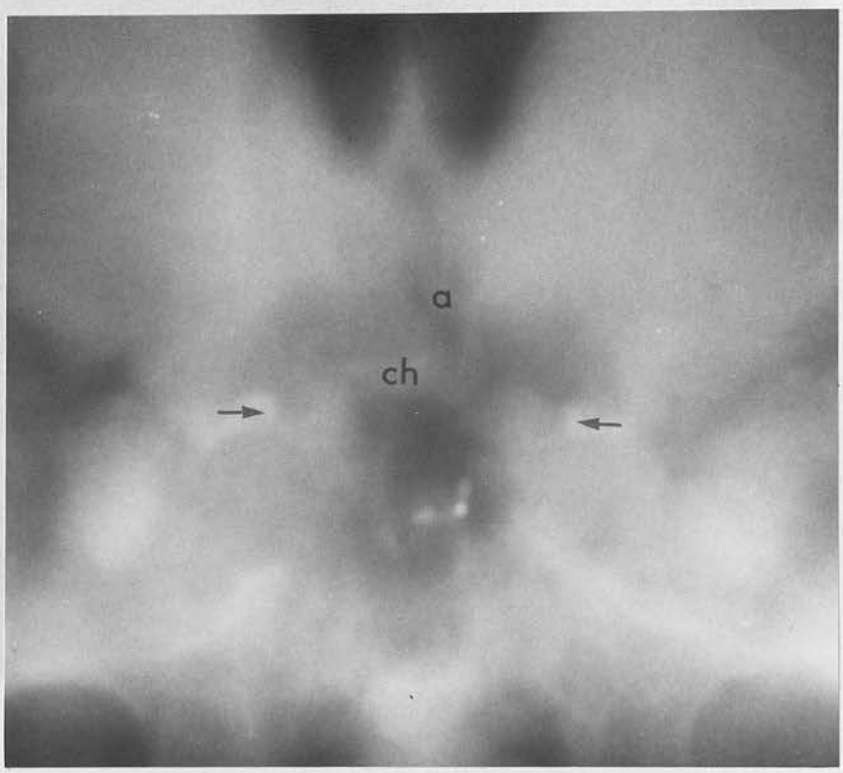

Figure 51 (cont.)

(c) Same patient (R. W.). Coronal plane. The presence of intrasellar gas is confirmed. Transverse arrows mark the anterior clinoids. The optic chiasm, which has remained in normal position, is indicated (ch). Visual fields were normal. No leakage of cerebrospinal fluid occurred. The left anterior cerebral artery (a) is also shown.

Figure 52

Patient with acromegalic giantism (D. R.). Sagittal plane. The tuberculum (on the left) and the tip of the dorsum are marked by tailed arrows. The superior surface of the gland (marked by arrowheads) is sunken within the sella. Patient had no history to suggest pituitary infarction and had received no previous local treatment to the pituitary. An anterior cerebral artery is indicated (a). The optic chiasm (unmarked) lies behind it and crosses it obliquely. A sella of this shape, wide superiorly, might be regarded by some observers as an indication of suprasellar extension. Hanging head autotomography did not demonstrate intrasellar gas.